UiT The Arctic University of Norway

Department of Electrical Engineering

Study & Analysis of Power Switches with reverse voltage blocking capability

Babur Zaman Khan Mughal
Candidate #: 8

Master's thesis in Electrical Engineering…ELE-3900-1 21V…May 2021

Acknowledgement

First, I thank Allah Almighty who gave me strength and knowledge to complete this thesis. The truth is, I could not have achieved this success without my mentor's guidance. But before that, I would like to thank my parents, who are always there to support me, unconditionally love me, and undoubtfully understand me. Along with them, I would like to thank my supervisors, Assistant Professor Trond Østrem and PhD researcher Umer Sohail who helped me in every step along the way whenever I needed their guidance. I would like to specially thank Assistant Professor Bjarte Hoff, PhD candidate Hussein Al-Sallami and Adeel Yousuf who have been there whenever I needed their help and guidance throughout my Masters studies.In the end I would like to thank the Department of Electrical Engineering in UiT Narvik for granting me access to their labs over the course of my thesis. I thank all people who put all the hard work and efforts into achieving the results. Thank you all for your unwavering support.

ABSTRACT

This thesis hovers over the basic introduction to Silicon Carbide (Metal Oxide Semiconductors Field-effect Transistor) MOSFET switches and the circuit designing of Current Source Invertors using SiC MOSFET switches. The thesis covers the basic grounds for all the steps needed in the implementation of hardware design for half bridge, full bridge and three phase CSIs in the future. Firstly, a detailed literature review is presented to give a deep knowledge about the importance and advantages of using SiC switches and CSIs. Furthermore, a comparison is taken between half bridge and full bridge voltage source converters alongside half and full bridge CSIs using (Physical security information management) PSIM software to model the circuits and analyze different aspects with respect to efficiency of both type of converters. The converters are compared with respect to different input voltages, frequency, and power. Afterwards, a fully working three phase Current Source Inverter is designed using Simulink platform and tested on different frequencies and the results are shown with the outputs of current and voltage waveforms. In the next step Simulations for the PCBs of half bridge, full bridge and three phase CSIs are simulated using LTspice software and examined with the desired output and then are designed in Easy EDA software ready to be printed. Lastly, an additional objective is achieved by testing the Cree's N-channel 3rd generation SiC MOSFETs (C3M0040120K) with Cree's gate driver CGD15SG00D2SiC in simple hardware circuits to observe their basic behavior. The results are shown using oscilloscope graphs against different voltages and currents. The whole dissertation is about the SiC switches, their working, specifications, usage, CSIs, and a lot more with simulations.

Table of Contents

List of Figures

List of Tables

ABBREVIATION

AC	Alternating Current
C	Carbon
CFFB	Current-Fed Full-Bridge
CFHB	Current-Fed Half-Bridge
CKT	Circuit
CRO	Cathode Ray Oscilloscope
CSC	Current Source Converter
CSI	Current Source Inverter
DC	Direct Current
EMI	Electromagnetic Interference
FET	Field Effect Transistor
GaAs	Gallium Arsenide
GaN	Gallium Nitride
GTO	Gate Turn-Off
HVDC	High Voltage Direct Current
IGBT	Insulated Gate Bipolar Transistor
IGCT	Integrated Gate Commutated Thyristor
I-V	Current-to-Voltage
JFET	Junction-Gate Field-Effect Transistor
LED	Light Emitting Diode
MOS	Metal-Oxide Semiconductor
MOSFETS	Metal-Oxide Semiconductor Field-Effect Transistor
MTBF	Mean Time Between Failure
NASA	National Aeronautics and Space Administrations
PCB	Printed Circuit Board

PEG	Polyethylene Glycol
PSIM	Physical Security Information Management
PWM	Pulse Width Modulation
RB	Reverse Blocking
SBD	Schottky Barrier Diode
Si	Silicon
SiC	SiC
SIT	System Integrating Testing
SMES	Semiconductor Magnetic Energy Storage
SVM	Support Vector Machine
UPS	Uninterruptable Power Supply
VFFB	Voltage-Fed Full-Bridge
VFHB	Voltage-Fed Half-Bridge
V-I	Voltage-to-Current
VSC	Voltage Source Converter

1. INTRODUCTION

Among many solid-state electronics applications, power electronics majorly deal with the conversion and control of electric power. Power electronics converters include inverters, rectifiers, DC-DC converters, and AC-AC converters. The CSIs are emerging as one of the new faces of converters due to their many advantages including low switching losses and over current protection. All the materials like Silicon (Si), Gallium Arsenide (GaAs), and many others are reaching their theoretical limits, and their place is taken by SiC , also known as Carborundum [1]. It is a semiconductor that comprises Silicon (Si) and Carbon (C). It is present in earth's crust in the form of a scarce mineral named moissanite. It is later synthesized and used for different purposes. After its manufacturing and its first use, it seems to be a revolutionizing element that can upgrade power electronics.

Among many modern and traditional switching devices, the SiC switches have emerged with unique properties and applications. They are becoming one of the crucial parts of power devices of the emerging world with their fast switching and fewer switching losses characteristics. These economical, practical, and compact semiconductor devices are well-known for their potential to reduce the end-product size significantly.

1.1. PROBLEM STATEMENT

With the increasing demand in renewable sector, Power electronic converters made of semiconductor power switches, are becoming more important due to the increased penetration of renewable energy sources and electrification of transportation sector. Power electronic converters can be divided into two types namely voltage-source converters and the current-source converters. Voltage-source converters are traditionally used in the previous years. However, the current-source inverters offer simplicity in the structure, low switching dv/dt and reliable overcurrent/short-circuit protection but they have not been well explored. One obstacle in the adoption of current-source inverters is their need for reverse-voltage-blocking switches. Recent advancement in wide-bandgap in SiC MOSFETSs have opened new possibilities for building reverse-voltage-blocking switches so further research is required. In power electronics, some switching devices like Si- IGBTs, Si-MOSFETs, and many others have worked efficiently for many years and they deliver quality output when used in any circuit. But the circuit in which they are used, have some limitations due to some conditions. They deliver good outputs, but they fail to operate effectively when used for high power high frequency operating circuits in demanding conditions over recent years. They cause more power losses with respect to SiC MOSFETs due to which the researchers and engineers were looking for their replacement. As a result, the SiC emerged as an effective switching device tending to operate at high power. It has lower On-state resistance and has low switching power losses due to which it is used in many applications, especially in power modules (supplies). It is not suitable for reverse blocking when operating at

high power. For this, different topologies of SiC MOSFETSs switches can be used for example common source or common drain mode.

The SiC MOSFETs based CSIs are used in many circuits that operate at high power, handle reverse blocking voltage, have low resistance, with low power and switching losses. The thesis comprises the three primary applications of SiC MOSFETs based CSI: half-bridge, full-bridge, and three-phase inverter circuit. These applications are discussed in further sections with their circuits, working, simulations, PCBs. The results prove the effective working of SiC MOSFETs based CSI.

1.2. SCOPE OF THE THESIS

The thesis is comprised of several sections. These sections are based on theoretical, experimental or both. They are presented in the thesis as mentioned below.

- The 1st section introduces the whole thesis and its main components like SiC and CSIs. It also presents their physical characteristics based on which they differ from other components. The section also involves the thesis's scope.
- The 2nd section comprises the literature review related to the SiC and CSI. It includes their history, working, applications, limitations, and many more.
- The 3rd section presents the comparison between half bridge and full bridge VSC & the half bridge and full bride CSI using PSIM software.
- The 4th section deals with the designing of three phase CSI in Simulink.
- The 5th section deals with the theoretical background of different topologies of SiC switches for reverse voltage blocking and circuit diagrams for half, full and three phase CSI.
- The 6th section encompasses the half-bridge, full-bridge, and three-phase inverter circuits' simulations and PCB designs. The results in this section are simulated using LTspice software and PCBs are created with Easy CAD software.
- The 7th section includes the hardware that consists of C3M0040120K based SiC MOSFETS and its gate-driver CGD15SG00D2. The section emphasizes the hardware designing, testing, and simulation results through an oscilloscope and presents all the details.
- The 8th section concludes the thesis work along with the future scope.

2. LITERATURE REVIEW

Early power electronics devices were very different from what they are now. Every device and component is getting better and better with the help of modern research. Similarly, the SiC or carborundum was a revolutionary change to power electronics. The SiC is silicon and carbon-conceived semiconductor since the late 1800s. This section presents the background, introduction, working, importance, applications, advantages, disadvantages, limitations, challenges of SiC with reverse voltage blocking CSIs.

2.1. HISTORY OF SiC MODULES

Before the invention and recognition of SiC, some lesser recognized and non-systematic experiments were performed, which includes the following [2]:

- In 1849, an electric current was passed through a sand-embedded carbon rod by Cesar-Mansuete Despretz.
- In 1881, silica was dissolved in a graphite crucible filled with molten silver by Robert Sydney Marsden.
- In 1881, a mixture of silica and silicon was heated in a graphite crucible by Paul Schuetzenberger.
- In 1882, silicon was heated under the stream of ethylene by Albert Colson.

A total of 0.03% carbon and 28% silicon comprises the earth's crust, but the SiC naturally occurs in the form of Moissanite [3].

2.1.1. MOISSANITE

Moissanite is the powered form of SiC rarely found in earth crust [4]. Later, they evolved as the element that can operate at high voltage and temperature and can be shaped as a device.

SiC was discovered in 1891 while producing artificial diamonds [5]. It was found in a research for a unique cutting and polishing material to substitute the luxurious diamonds. A synthetically produced complex chemical compound was important for cutting tools and grinding wheels. It was used in LEDs in 1907 and later in lightning arresters [6].

Since then, SiC has become a significant part of power electronics because of its extensive use in different fabrications, manufacturing, high-frequency requirements, and many more. Along with the SiC, the CSIs with the reverse blocking voltage uses SiC modules for different power modules. The one used in the thesis is among them.

2.2. Silicon Carbide

SiCs are crystalline compounds that are synthetically produced from the mixture of silicon and carbon. They were discovered in the late 19^{th} century, and their chemical formula is SiC. Some of the critical materials in which the SiC was used after manufacturing were cutting tools, sandpapers, and grinding wheels. *Figure 2.1* shows the synthesized SiC.

Figure 2-1: SiC

SiC is among those wide-gap semiconductors used in high-power applications [7]. Some of the physical and chemical properties of SiC are stated in the *Table-2.1*.

Table 2.1: Physical and Chemical Properties of SiC [7]

Sr. No.	Properties	Statistics	Unit
1.	Density	3.02	g/cm^3
2.	Color	Black	-
3.	Bending Strength	At 20 °C; 250	Mpa
		At 1200 °C; 280	
4.	Hardness	2800	Kg/mm^2
5.	Fracture Toughness	4.6	-
6.	Mohs Hardness	13	-
7.	Open Porosity	< 0.1	%
8.	Operating Temperature (Maximum)	1380	°C
9.	Elastic Modulus	At 20 °C; 330	Gpa
		At 1200°C; 45	
10.	Thermal Expansion Co-efficient	4.5	$K^{-1} \times 10^{-6}$
11.	Melting Point	2200 – 2700	°C
12.	Specific Heat	750	J/Kg °K
13.	Volume Resistivity	$10^2 – 10^6$	Ω – cm

Beyond all the characteristics and properties of SiC, the percentage effect of the weight of SIC's nanoparticles in addition to Young's modulus is presented in the following graph. This graph shows that with the increase in the percentage of SiC particles, the young modulus also increases [8].

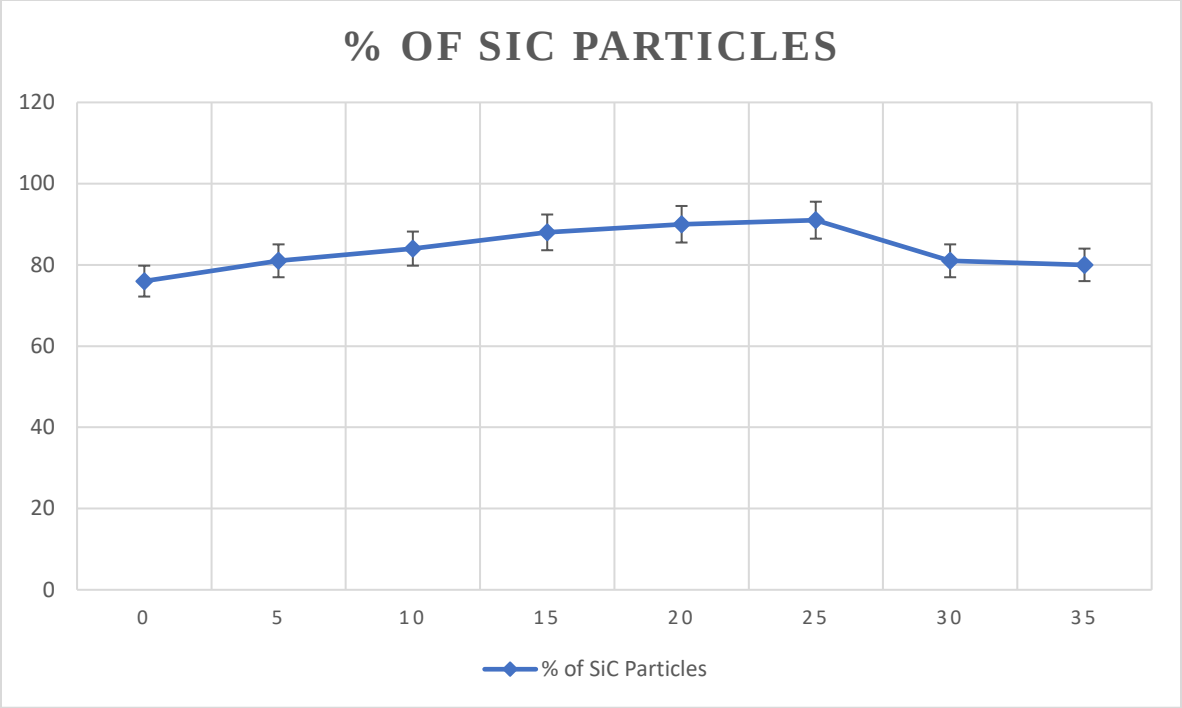

Figure 2-2: Percentage of SiC Particles to Young Modulus Graph [8]

The graph in *Figure 2.2* shows the performance of SiC particles that act as a reinforcement material on the mechanical properties of many alloys. The percentage fraction for efficiency increases with 5% difference for molten alloys, whereas SiC act as a complex, dense, and ultimate tensile material of greater strength when solidified.

Some of the SiC applications include:

- Automotive Water Pump Seals
- Ceramic and Electronic Components
- Extrusion Dies
- Float Glass Production
- Heat Treatment of Metals
- High Voltage Devices
- Igniters for Gas Heaters in Pilot Lights
- Melting of Glass and Non-Ferrous Metals
- Microelectronic Applications
- Optoelectronics
- Pump Components
- RF Power Devices
- Sandblasting Ignitors
- Sensors
- Switching Power Devices

SiC technology is used in many fast-switching & high powered devices. These devices are discussed in further sections.

2.3. SiC SWITCHES

The switches that specify having high-frequency capabilities are in much demand in electronics. The SiC switches are one of the low-loss semiconductors with many characteristics [4] like:

- Superior high temperature
- High-voltage performance
- Low ON-state resistance
- High-frequency switching
- Less switching losses

The SiC material is better than the material that were used before the SiC for switching in power devices. Physical characteristics and properties-based comparison table among different power devices technologies are displayed as follows (see *Table-2.2*).

Table 2.2: Physical Characteristics and Properties Comparison [9] [10]

Sr. No.	Properties	GaN	GaAs	Si	SiC	Unit
1.	Crystal Structure	Hexagonal	Zincblende	Diamond	Hexagonal	-
2.	Thermal Conductivity	1.3	0.5	1.5	4.9	W/cm
3.	Energy Gap	3.5	1.43	1.12	3.26	eV
4.	Breakdown Field	3	0.4	0.3	3	V/cm x 10^6
5.	Drift Velocity	2.7	2	1	2.7	cm/s x 10^7
6.	Relative Dielectric Constant	9.5	12.8	11.8	9.7	-
7.	Electron Mobility	1250	8500	1400	900	cm^2/V_s

8.	Hole Mobility	200	400	600	100	cm^2
9.	Relative Permittivity	9.5	13	11.9	10	-
10.	Central Electric Field	3	0.3	0.25	2.2	$MV\ cm^{-1}$

The above-stated properties separate the SiC from the remaining materials in making efficient and compact power converters for higher voltages & currents. The greater width of the SiC's energy bandgap leads to a higher junction temperature that limits the leakage current to a minimum in blocking mode [9]. This means that the SiC-based switches can operate at a high temperature with less risk of leakage current or losses. Also, the thermal conductivity of SiC leads to a high percentage of heat getting removed from the junction [10]. The high drift velocity of SiC offers electrons to move fast in SiC devices that will gradually increase the switching speed and introduces the possibility of operating at high frequency. Thus, the SiC switches are more efficient in reducing power and switching losses while operating at high frequencies irrespective of voltage and current overshoot [11].

SiC is mostly unipolar devices used due to low hole mobility [12]. They are the majority charge carrier devices that do not inject the minority charge carrier. Some SiC technology-based unipolar devices include the (MOSFETSs), Junction-gate Fields Effect Transistors (JFETs), and System Integrating Testing's (SITs) [13].

If the Silicon (Si) and SiC are compared based on the specific ON-resistance versus breakdown voltage, the following graph is achieved [14].

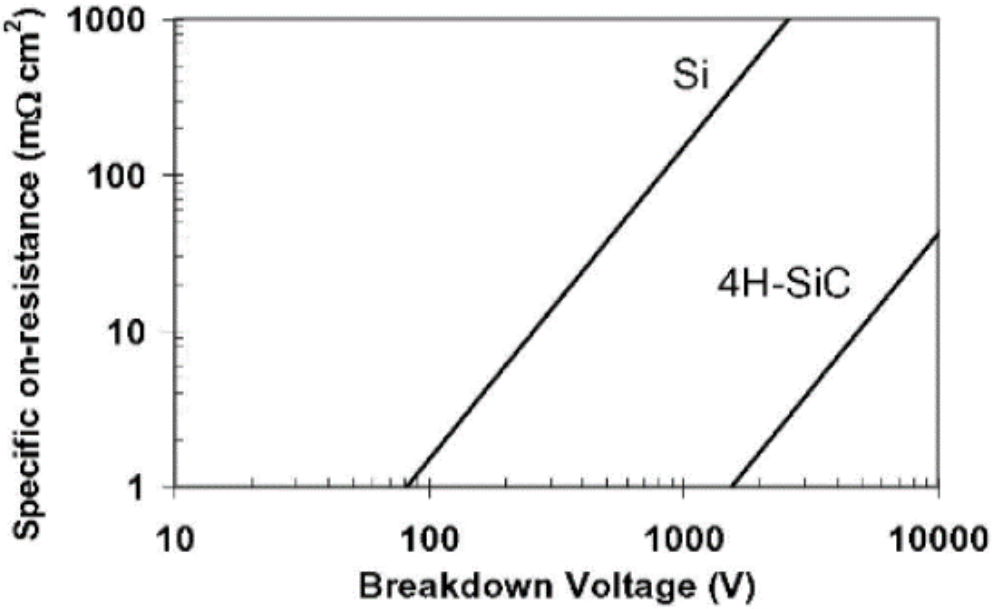

Figure 2-3: On-Resistance versus Breakdown Voltage of Si and SiC [14]

Some of the applications of SiC technology include the following.

- Power converters for electric and hybrid vehicles

- High-voltage switches for X-ray generators
- High-efficiency inverters in DC/AC converters for solar and wind power
- Thin-film coating processes
- Power inverters for industrial equipment and air conditioners

Among many SiC switching devices, the SiC Schottky Barrier Diode (SBD) and SiC MOSFETSs are the most efficient and less switching losses even at high frequencies. They are discussed as follows:

2.3.1. SiC SCHOYYKY BARRIER DIODE (SBD)

SiC technology-based SBDs are freewheeling and fast switching diodes with low threshold voltage and excellent reverse recovery dynamics [15]. They are mostly independent of the transistor drain current and lead to less power loss. These diodes are formed by the thin aluminum contact with the n-type semiconductor, where aluminum act as anode and the n-type semiconductor is the cathode. The cross-sectional view of SBD is shown in *Figure 2.4*.

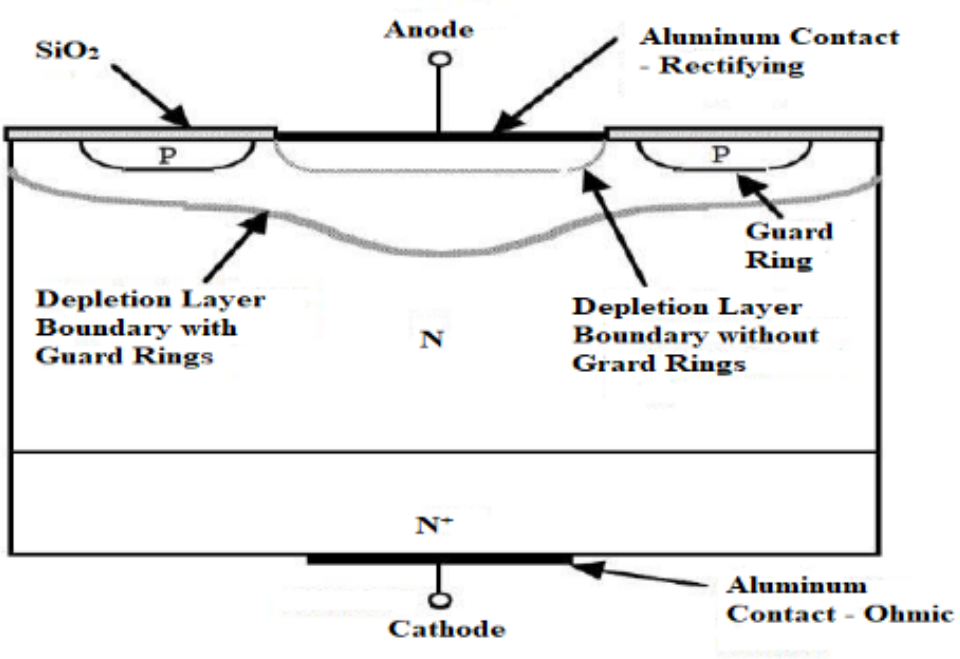

Figure 2-4: Cross-Sectional View of SiC-Based SBD [15]

They form the depletion layer boundary without guard rings at aluminum contact that must perform rectification. The SBDs are majority carrier devices with the following I–V characteristics curve.

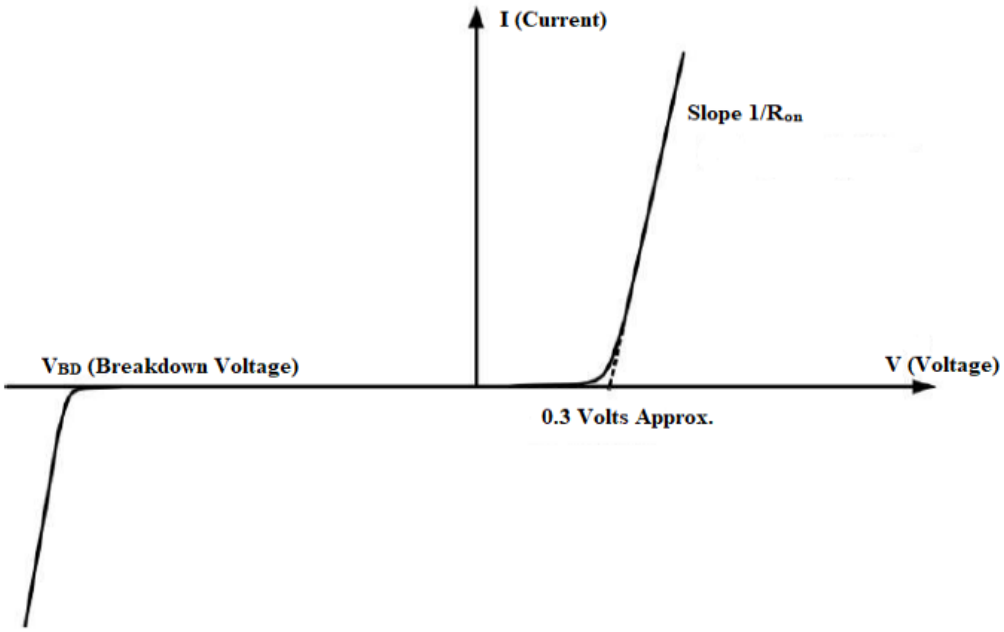

Figure 2-5: I–V Characteristics Curve of SiC-Based SBD [15]

The R_{on} can be calculated using the following formula.

$$R_{on} = \frac{4\,V_B^2}{\varepsilon\,\mu_n\,E_C^3}$$

The I–V Characteristics curve shows that the ON-state threshold voltage will be less than the threshold voltage of the PN-junction diode. The reason is that many charge carrier devices are required to remove the stored charge from the drift region before switching OFF the diode [16].

2.3.2. SiC MOSFETs

The SiC MOSFETs have hard-switching and fast-switching transients far better than Si power MOSFETSs and Si IGBTs [17]. The previous technologies have many voltages and current overshoot challenges that can be overcome with the snubber circuit that helps in the reduction of stress from the transistor during switching [18]. A snubber circuit helps in suppressing the voltage ringing in SiC-based half-bridge circuits [19]. et al. proved that the RC turn-off snubber circuit is the best solution for reducing acceptable level switching stress on power devices [20][21].

The SiC MOSFETSs have superior properties as compared to other switching devices. It differentiates based on the following properties [22]:

- Fast switching transients
- Good thermal properties
- High blocking voltage

- Low switching losses
- Low ON-state resistance

Figure 2.6 displayed below depicts the capabilities of SiC MOSFETSs on other switching devices.

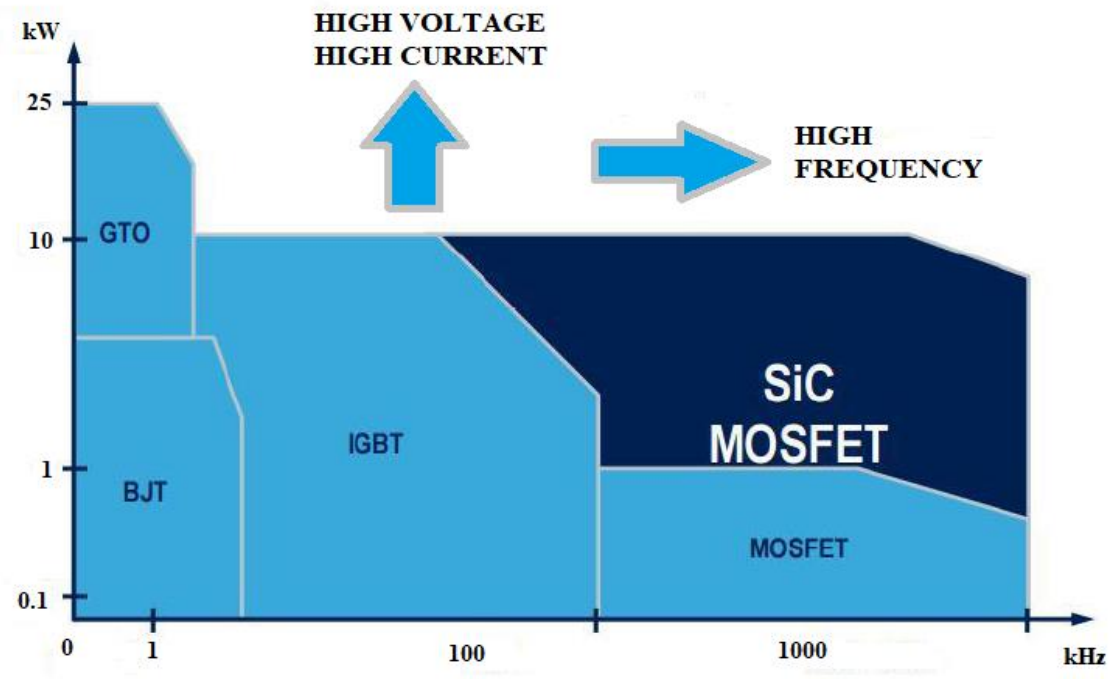

Figure 2-6: Leading Capabilities of SiC MOSFETSs on Other Devices [22]

SiC MOSFETSs comprises four terminals that are Drain (D), Source (S), Body (B), and Gate (G). The MOSFETSs are designed so that the Gate terminal controls the flow of current These MOSFETSs are divided into two types, a D-MOSFETS and E-MOSFETS, whose fundamental difference is stated as follows [23]:

- In Double Implanted MOSFETS (D-MOSFETS), the n-type semiconductor exists between the source and drain by default (placed during construction).
- In Enhancement-Mode MOSFETS (E-MOSFETS), n-channel does not exist between source and drain.

The basic structure of an N-channel MOSFETS is shown in *Figure 2.7*, whereas I–V characteristic curve of the SiC MOSFETS is presented in *Figure 2.8*.

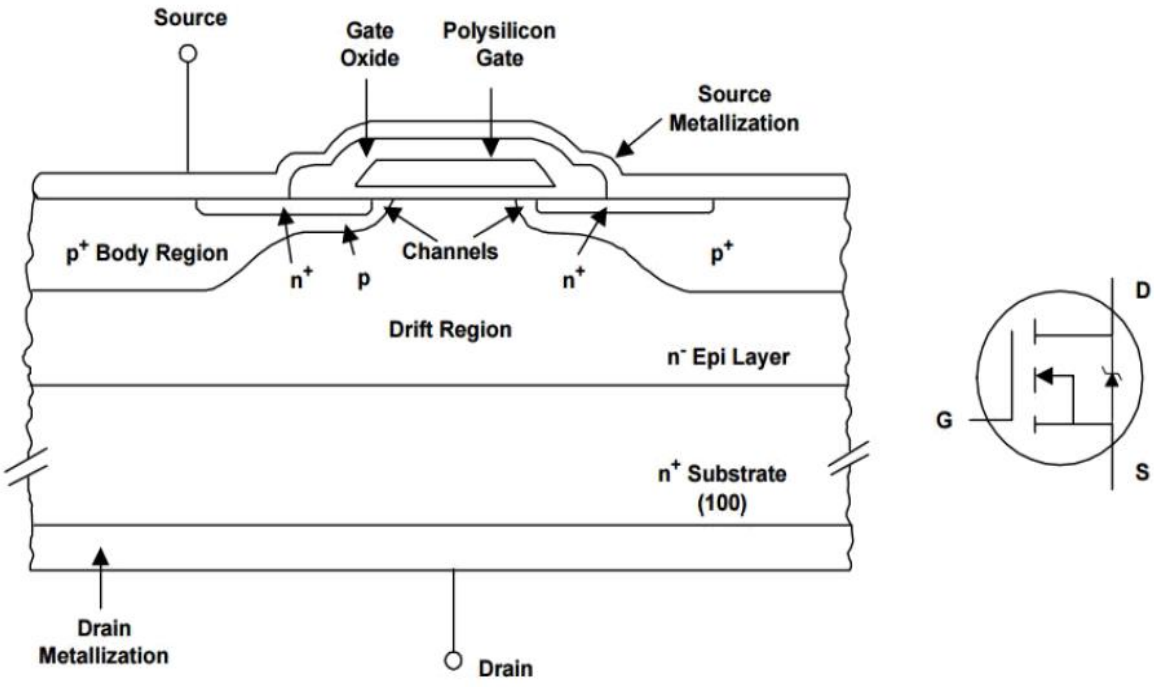

Figure 2-7: Basic Structure of N-Channel MOSFETS [24]

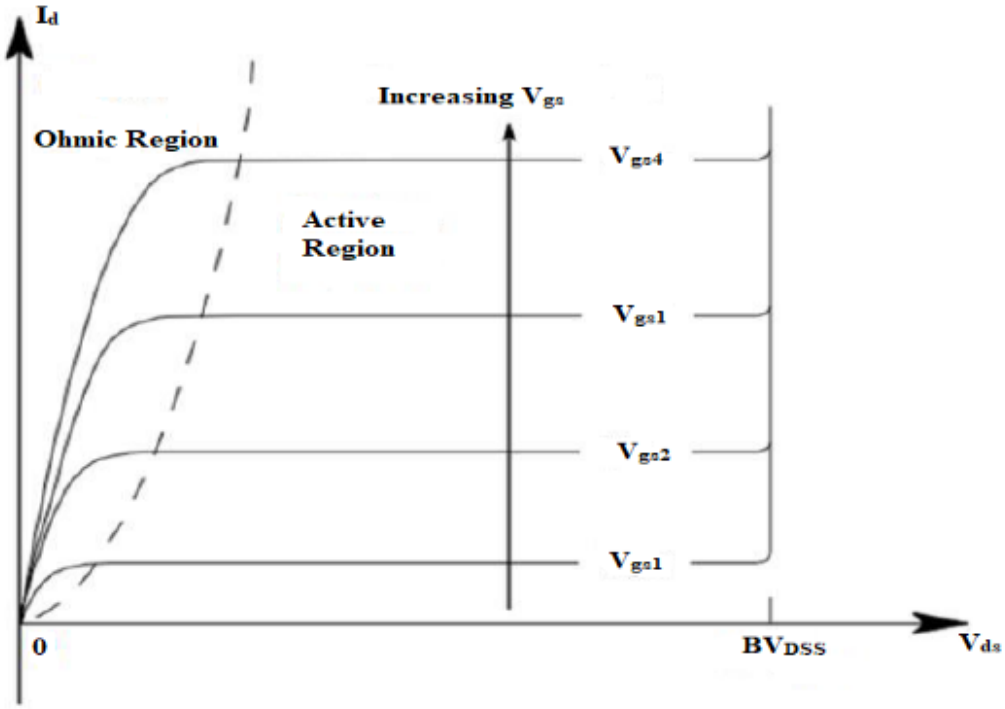

Figure 2-8: I–V Characteristic Curve of the SiC MOSFETS [25]

It can be observed from the I–V characteristics curve of the SiC MOSFETs that the ON-state drain-to-source resistance has a significant impact on gate-to-source voltage. Also, it can be said that:

$$ON - State\ Resistance\ of\ MOSFET \propto \frac{1}{|Positive\ Bias\ Gate - to - Source\ Voltage|}$$

There will be no drain current for low gate-to-source voltage because of the low field effect that cannot induce conduction between source and drain. The SiC MOSFET's switching transient characteristics can be examined in a buck converter whose turn-on characteristics are shown in *Figure 2.9*. The transient switching is without diode recovery [26].

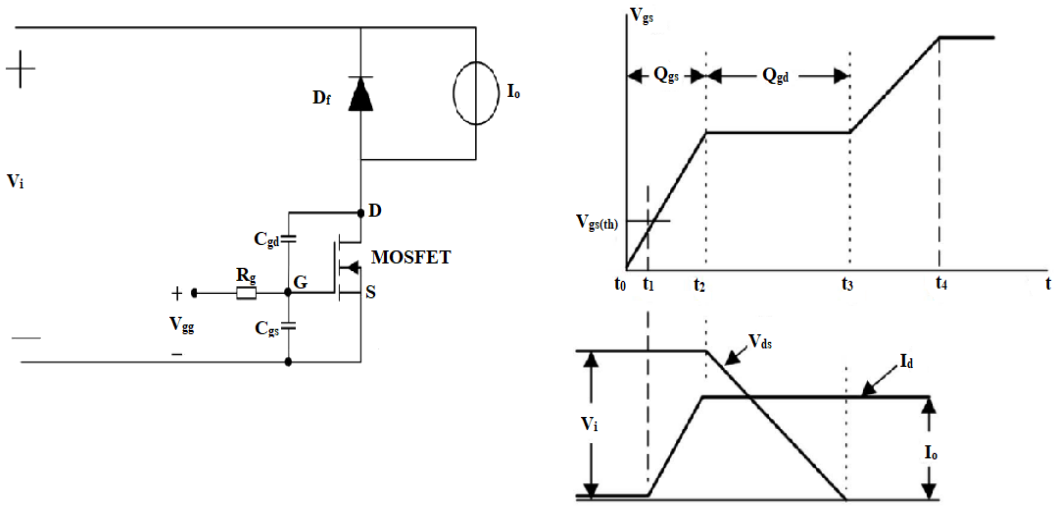

Figure 2-9: Switching Transient Characteristics of SiC MOSFETS in Turn-On [26]

Some of the crucial parameters of the SiC MOSFETs are listed in *Table-2.3*.

Table 2.3: SiC MOSFETS Model Parameters [26]

Sr. No.	Parameters	Statistics	Units
1.	Threshold Voltage (V_{TH})	5.86	V
2.	Drain-to-Source Voltage (V_{DS})	1200	V
3.	Wavelength (λ)	0.04647	V^{-1}
4.	Resistance (R_{DS})	450	mΩ
5.	Power Dissipation	85	W
6.	Operating Junction Temperature	175	°C

2.4. CURRENT SOURCE CONVERTERS

Many power devices face the issue of switching losses at higher frequencies and high temperatures. To overcome this, the power converters are used along with some passive components to reduce losses [27]. The power converters or have switching transients with low EMI and little ranging, or low voltage and current overshoot on which the distribution system's power quality relies. But power converters are not much efficient. They are the reason for substantial power loss during the fast switching at high frequencies. Moreover, the converters based on earlier technologies like Silicon (Si), either Si IGBT-based converters or Si power

MOSFETSs-based converters, remain no more efficient and reach their theoretical limits [28]. Thus, the SiC technology is taking place along with the CSIs and converters, which are highly efficient and tend to operate in high temperatures, and high frequencies while delivering minimum power and witching losses.

CSIs are more reliable and better than voltage source converters [29]. *Figure 2.10* shows the circuit diagrams of current and voltage source converters.

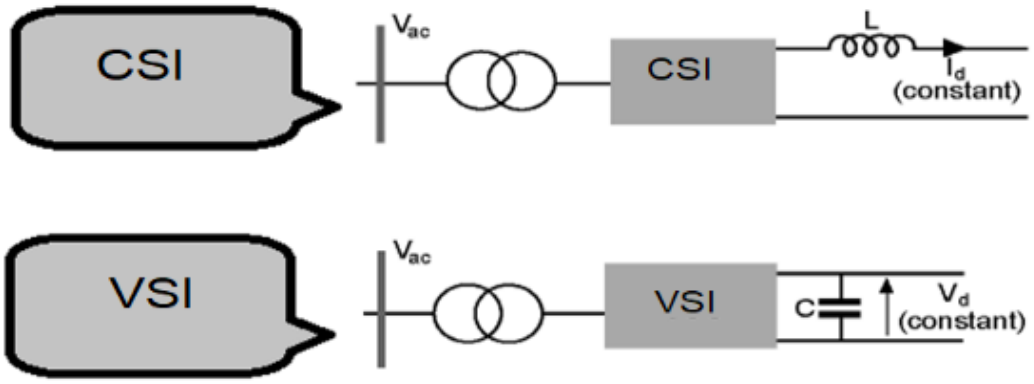

Figure 2-10: Current Source and Voltage Source Inverter Circuits [29]

Table 2.4: Comparison between Current Source and Voltage Source Inverters [29] [30] [31]

Sr. No.	Current Source Inverters (CSI)	Voltage Source Inverters (VSI)
1.	DC-side current maintains the same polarity	The converter itself keeps the same voltage polarity
2.	More reliable	Less reliable
3.	Drive better Mean Time Between Failure (MTBF) rate irrespective of the number of the components	Drive better Mean Time Between Failure (MTBF) rate with fewer components
4.	More efficient with SiC switching	More efficient with IGBT switching
5.	The communication circuit is simple and comprises capacitors	The communication circuit is complicated
6.	It does not require any feedback diodes	Require feedback diodes
7.	Input voltage is maintained at constant but adjustable	Input voltage is maintained at constant
8.	The output voltage depends on the load	Output voltage does not depend on the load

An experiment was performed for the evolution of the performance of power DC/DC boost converters and achieved 99.3% efficiency through SiC MOSFETs at 100 kHz frequency and got an 18% reduced power loss [30]. This means the SiC switches in contact with the converters for

decreased power and switching losses. The SiC switches can be used in many applications and the CSIs like the half-bridge, full-bridge, three-phase power modules, and many more.

SiC JFET and CSI-based power electronics module works on 200 kHz frequency and generates 1200 Volts, 6 Amps with a capacitor in DC-Link topologies [31]. Similarly the SiC MOSFETs with voltage source inverters tend to generate 1.7kV and 3.3kV up to 2MW but can cause a decrease in results and efficiency in the case of short circuits [32]. Thus, the 1700 Volts, 300 Amps was generated with SiC MOSFETs and CSIs with two different DC-link stray inductances of 30nH and 100nH at two different temperatures that are 25 °C (room temperature) and 125 °C. Thus, a high voltage output, switching efficiency, and reduction in power and switching losses can be achieved with the SiC MOSFETs and CSIs.

2.5. INTRODUCTION TO SiC AND REVERSE BLOCKING CSIs

A semiconductor containing a specific percentage of silicon and carbon generates Carborundum or SiC (SiC). It is a sporadic appearance in nature but is very useful. The SiC semiconductors operate at high voltages and high temperatures irrespective of their size. Maurizio highlighted the importance of the SiC MOSFETSs that dramatically improve power electronics and power systems with their switching capabilities [33]. Insulated Gate Bipolar Transistors (IGBT) technology that emerged in the 1980s provides high-efficiency performance and cost-efficiency to the power converters but can not handle the switching losses.

The SiC technology maintains the voltage blocking capability and reduces the switching losses while providing an efficient output even with a smaller size. The SiC is of hexagonal crystal structure, with a 3.26 eV energy gap, 900 cm^2/V_s electron mobility, 100 cm^2 hole mobility, 4.9 W/cm thermal conductivity, 2.7 x 10^7 cm/s saturation drift velocity, and 9.7 e_s relative dielectric constant [33].

A CSI-based single conversion stage method was introduced for the three-phase power electronic interface photovoltaic implementation [34]. The cost-effective and independently controlled CSIs topology for the DC sources, as a replacement for the DC/DC converter, was also proposed that showed high working efficiency. CSIs have reverse-blocking features that sometimes require some modules like SiC modules.

The SiC MOSFETSs was introduced as a dramatic improvement upon existing silicon devices highlighted its working for the CSIs with zero-voltage switching [35]. The modulation strategies were also addressed for the solid-state transformer voltage stress at different rated voltages (1.5kV, 10 kVA).

SiC switches or switching devices are best suitable with the CSIs. The CSIs sometimes are used with reverse voltage blocking, whereas sometimes they are used for active power decoupling. The limitations of low frequency-based power oscillations of DC side single-phase converters presents the active power decoupling technique with the CSCs in improving the power oscillations issue [36].

The model of the synchronous reverse blocking switches with CSCs and a soft-switching-based solid-state transformer was presented that have minimized conventional reverse blocking characteristics as compared to the MOSFETS or IGBT based switches [37]. They have achieved 97.8% efficiency at 750 W delivery level power.

Thus, it can be observed from the above works of literature that SiC is a semiconductor device that is suitable for switching purposes even at high frequency with more minor switching losses. But some oscillations or harmonics are generated that are needed to be suppressed. For this, the CSIs and converters are the best choice. These devices are thoroughly explained below under the observation and experience of already presented pieces of literature.

2.6. SiC MANUFACTURING

SiC rarely occurs in an earth's crust but not in its pure form but the highly scarce form of Moissanite. Most synthetic can be later used as semiconductors or gem-quality diamond simulants [38]. Among many methods, the simplest one is to take an Acheson graphite electric resistance furnace and combine carbon with silica sand in it at high temperature of about 1600°C and 2500°C that is 2910°F and 4530°F, respectively [39].

A new process has emerged for nanometric SiC production through the freeze-dried gel's carbothermal reduction method [40]. To get a considerable large size SiC particle, the temperature is adjusted to 1400°C.

A Ley process is also an effective way to make pure SiC by subliming the powered SiC into an argon gas 2500°C high-temperature species of carbon, silicon, SiC (SI_2C) and Silicon dicarbide (SiC_2) [41] [42]. The manufactured SiC is then cut down into wafers using the laser, or diamond wire saw. These wafers are used extensively in power electronics.

2.7. PROPERTIES OF SiC SWITCHES

SiC (SiC) acts as a power device that can work with high frequency delivering fast switching with minimum losses. If the SiC is compared with Si, the properties, and technical details that we get are as follows:

- The breakdown field is 10 times stronger in SiC than in Si.
- The maximum thermal conductivity of SiC ranges from 3.3 to 4.5 W/cmK compared to Si, which has a higher thermal conductivity of 1.5 W/cmK.
- The bandgap of SiC is 3 times greater than that of Si.
- The thinner epitaxial layers are 10 to 20 times more than that of Si.

If the performance of the SiC is examined, we have the following details.

- 2 to 3 times lower on-state voltage drop as compared to other switches.
- About 100 to 1000 times faster-switching speed
- Shallow leakage current

- High chip temperatures approximately 250 - 300 °C instead of 125 °C that is common for every chip
- 3 to 10 times higher intrinsic adiabatic pulsed current level

The impact that SiC power switches have on other power circuits are stated as follows:

- Compact circuits
- Higher efficiency in circuits
- High-temperature operation
- Higher pulsed power
- Higher continuous current densities
- Higher current capability
- Compatible with CSCs
- Cost-efficient

2.8. WORKING OF SiC

SiC is a part of various semiconductor devices that perform fast switching while operating at high frequency with minimum switching losses. The switching processes can be performed using either SiC diode and SiC MOSFETs. These devices are best known for their working efficiency and reliability. SiC switches present low capacitive switching losses when compared to the Si switches. A 99.1% accuracy was achieved with half nominal load and 99% efficiency with a full nominal load while using SiC switches [43]. Moreover, the high efficiency switching properties remain the same for even the DC-DC boost stage where the blocking voltage is around 1200 – 1700 Volts enabling circuit controls and topologies. The working of SiC switching devices is stated as follows under the light of already presented literature.

2.8.1. SiC DIODE WORKING

SiC diodes work in a format that whenever anode is given positive voltage. The barrier potential formed by the depletion layer gets reduced, allowing the current to flow, generating the forward voltage slope at 0.3 Volts approximately [44]. While turning off the SiC diode, the current junction capacitance discharge is the reverse recovery current [45]. The reverse recovery current is independent of the transistor's drain current if the diode work as a freewheeling diode. This leads to 2/3 of low power, switching losses, and faster quick turn. Thus, the SiC diodes have current ratings of 40 Ampere approximately and voltage ratings of 1200 Volts approximately [45].

2.8.2. SiC MOSFETSs WORKING

The SiCs are low switching losses and time devices with no tail current because of which they are also called majority carrier devices [46]. Because of the wider bandgap present in SiC MOSFETs, the on-state resistance is much lower due to the smaller drift region. SiC MOSFETs are fast switching devices because they produce more oscillating transients along with the parasitic compared to other devices. This sometimes leads to voltage overshoot in the

converter circuit due to the produced parasitic [47]. The reverse voltage blocking circuit with the CSI can somehow depict high power and frequency capabilities.

The SiC MOSFET is conducted to flow from the drain terminal to the source terminal, and this flow is controlled by the voltage applied between the gate terminal and the source terminal. Suppose the positive voltage is inputted at the gate terminal. In that case, the channel's body is filled by the negative charges forming a conducting channel, allowing the majority carriers to flow from drain to source [48]. Thus, the device will offer fast switching without switching losses when the magnitude of drain-source voltage influences the drain current; the MOSFETS is said to be n the ohmic region [49]. No drain current flows for the low gate to source voltage because of the gate field effect that is not very high to induce conduction within the channel. However, the gate to source voltage increases at the threshold voltage and forms a conducting channel between gate and source.

2.9. ADVANTAGES OF REVERSE BLOCKING CSIS

Typical gate Turn-Off (GTO) thyristors' CSIs have an advantage over reverse blocking. They remove the reverse blocking diode for the reduction of the conduction losses [50]. This causes many current to flow backward through the gate turn-off thyristor during the reverse recovery process.

The voltage source inverters are advantageous among electrical drives, but the relaunch of CSIs has proven themselves more reliable and efficient [51]. Beyond the advantages, slow dynamic response and low speed are the disadvantages [52]. Moreover, it needs a different converter stage to work correctly.

2.10. LIMITATIONS AND CHALLENGES RELATED TO SiC USE

In the early 1990s, NASA was about to work with the SiC semiconductors and intended to the widespread acceptance of SiC instead of silicon. Still, they find some limitations in the actual fabrication of many devices [53]. In the 2010s, SiC grew effectively and became a genuine part of power electronics based on its vast characteristics. The significant impact of SiC on power electronics embraces higher switching frequencies, low resistance, extreme temperature tolerance, higher voltages, and a wider bandgap [53].

The device's reliability is challenging with SiC doping, SiC epitaxy, and SiC etching, which still need improvement to mature SiC technology in power electronics [54]. The new defects in epitaxial layers and wafers of SiC decrease the required breakdown electric field, which fallouts in increasing the leakage current and reducing the on-state device performance. It is observed that switching speed as a challenge in 10 kV SiC MOSFETSS due to heat sink, crosstalk, electromagnetic interference to the control, and stray inductance [55]. These limitations and challenges are needed to be entertained.

In the field of power electronics, the new technologies development has targeted the industrial market in the direction of the enhanced energy efficiency resources. The restricted

development of more minor switching losses and fast switching speed has led the technology toward the SiC [56]. SiC has wider bandwidth than the Si and can operate in high voltage and high frequency while providing minimum switching losses. They are given priority because of their switching ability, either because the switch is made up of SiC diode or SiC MOSFETs. It delivers highly efficient output irrespective of the input voltage and frequency. Thus, they are beneficial for the CSCs even with the reverse voltage breakdown conditions.

3. SIMULATIONS

This part of the thesis deals with the comparison of voltage source converters to the CSIs in different topologies with simulation results and comparisons of four conventional isolated converters: current-fed half-bridge converter (CFHB), current-fed full-bridge converter (CFFB), voltage-fed half-bridge converter (VFHB), and voltage-fed full-bridge converter (VFFB).

The simulations were performed on PSIM v9.1 utilizing the thermal modules of the semiconductors to get losses and efficiencies for each converter. The semiconductors utilized were the SiC Power MOSFETS SCTWA60N120G2-4 from STMicroelectronics and the ISL9R3060G2 Farchild. Semiconductors.

The converters were tested for different input voltages, frequencies, and power to verify the differences in voltage and current variations, as well as steady-state and transient losses. PSIM 9.1 was used in these simulations, software from Powers, and used for the simulations of different power electronics circuits with motor drives.

3.1. VOLTAGE-FED FULL-BRIDGE CONVERTER (VFFB)

Figure 5.1 shows the topology of the voltage-fed full-bridge converter. This converter has twice as many switches compared to the half-bridge topology. But it is possible to reduce the total number of semiconductors by utilizing a three-winding transformer, as shown in *Figure 5.1* [57]. Compared to the voltage-fed half-bridge converter, the full-bridge has a voltage gain twice as higher, requiring a lower duty cycle (D).

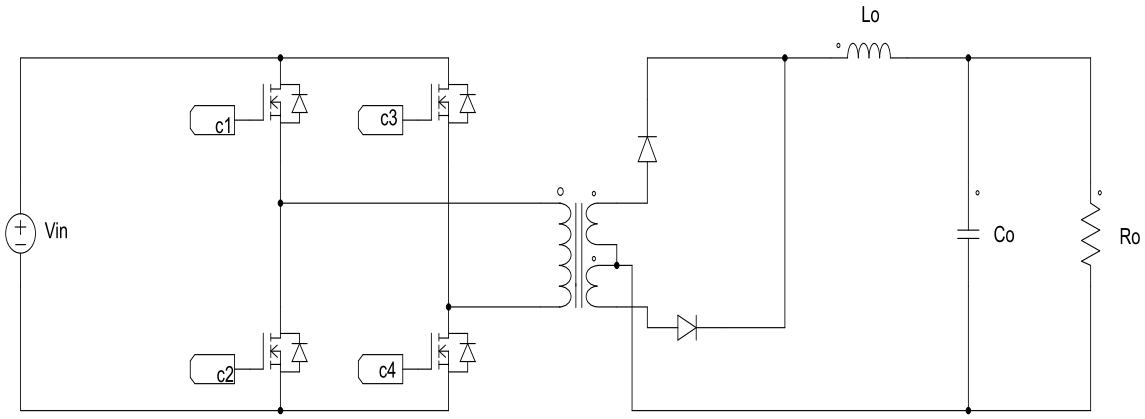

Figure 3-1: Voltage-Fed Full-Bridge Converter

3.1.1. SIMULATION SCENARIO 1

The following parameters were defined for the first simulation considering a battery charger application.

Table 3.1: Parameters for the First Simulation of the VFFB

Sr. No.	Parameter	Value
1.	Input Voltage (Vin)	600 V

2.	Output Voltage (Vout)	48 V
3.	Output Power (Po)	1000 W
4.	Transformer Ratio	4:1
5.	Cin	100 µF
6.	Lo	150 µF
7.	Co	22 µF
8.	Switching frequency (fs)	100 kHz
9.	D	0.16

Figure 5.2 shows waveforms output waveforms of the VFFB converter considering the parameters presented in *Table 5.1*. For these values, the current ripple in Lo was 1.10 A, the output voltage variation was 32.84 mV, and the current ripple in the load was 14.25mA for an output power of 1000 W. The Frequency of these ripples is equal to fs=100 kHz.

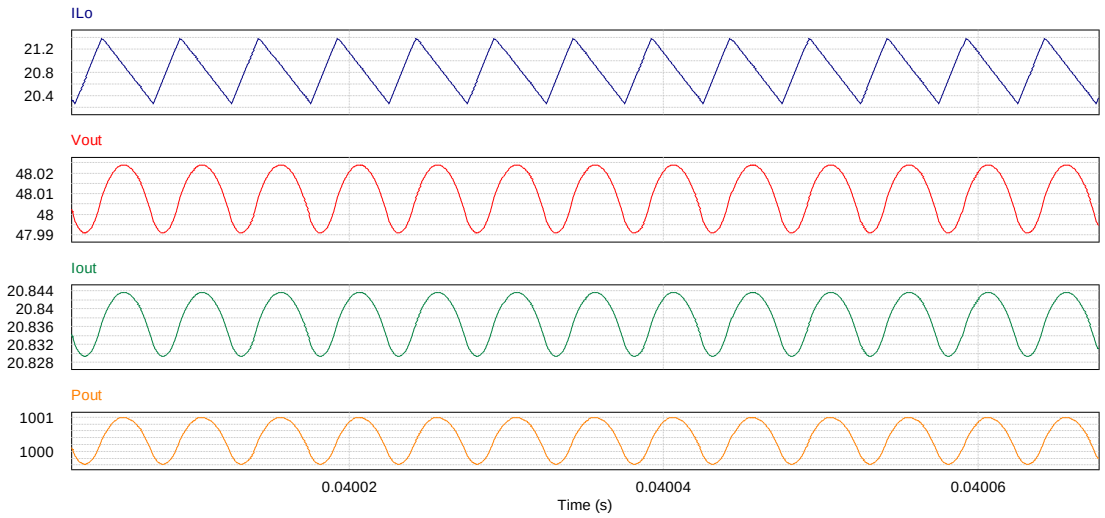

Figure 3-2: VFFB Output Waveforms for Table 5.1 Parameters

Regarding steady-state power losses, the conduction losses in the switches were 331mW, while the switching losses were 9.13 W, with no losses in the body diode. The losses in the rectifier diodes were 3.77 W for conduction and 17.33 W for switching.

When starting up the converter, peak transient losses in the switch were 494 mW for conduction and 10.71 W for switching. In the rectifier diodes, the peak losses reached 3.92 W for conduction and 21.91 W for switching.

3.1.2. SIMULATION SCENARIO 2

A second simulation is performed, reducing the frequency to 50 kHz and the input voltage to 415 V, which required a higher duty cycle (D) due to the voltage decrease.

Table 3.2: Parameters for the Second Simulation of the VFFB

Sr. No.	Parameter	Value
1.	Input Voltage (Vin)	415 V
2.	Output Voltage (Vout)	48 V
3.	Output Power (Po)	1000 W
4.	Transformer Ratio	4:1
5.	Cin	100 μF
6.	Lo	150 μF
7.	Co	22 μF
8.	Switching frequency (fs)	50 kHz
9.	D	0.23

For these parameters, the current ripple in Lo was 1.61 A, while the output achieved an oscillation of 40.76 mA and 93.78 mV for the current and voltage, respectively. The increased voltage and current oscillations are explained by the frequency reduction, which does not affect the voltage gain. But it also brings some benefits, such as lower switching losses.

The switching losses of the switches in steady-state were 3.02 W, and rectifier diodes released 22.37 W for a lower input voltage and frequency (415 V and 50 kHz). On the other hand, the conduction losses in the switches increased to 876 mW since the input voltage is lower and, in the diodes, these losses were 1.82 W.

During startup, the switching and conduction losses in the switches reached a peak value of 3.5 W and 1.25 W, respectively. In the diodes, the conduction losses reached 2.68 W while the switching losses 28.15 W.

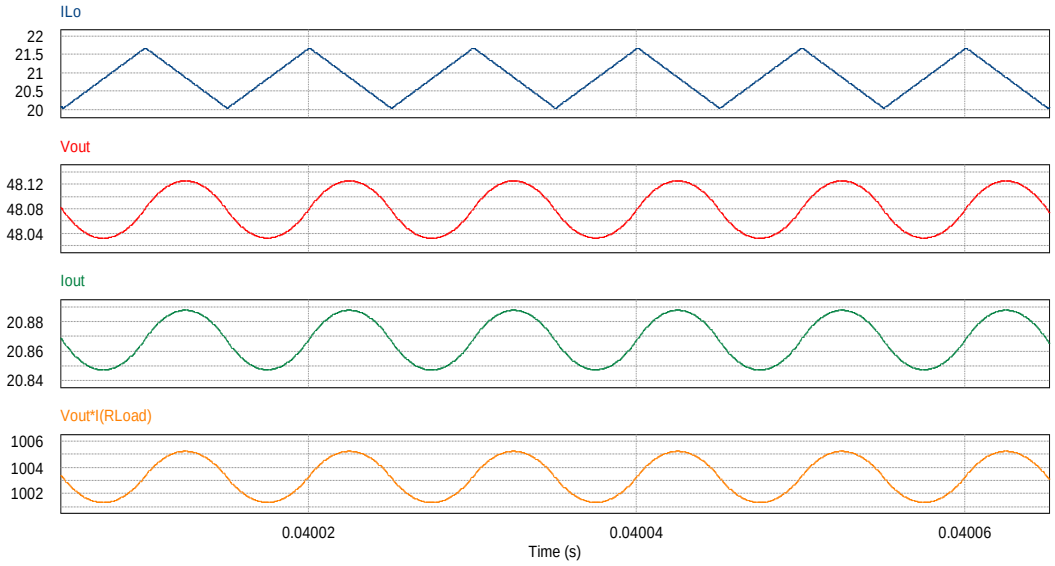

Figure 3-3: VFFB Output Waveforms for Table 5.2 Parameters

3.2. VOLTAGE-FED HALF-BRIDGE CONVERTER (VFHB)

In this voltage-fed topology, the input voltage is divided between capacitors C1 and C2, and the switches are driven complementary, creating an alternating waveform in the primary winding of the transformer. The significant advantage of this topology over the full-bridge is that it has half of the switches. But, its voltage gain is also decreased by half, requiring higher transformer ratios or duty cycle [58].

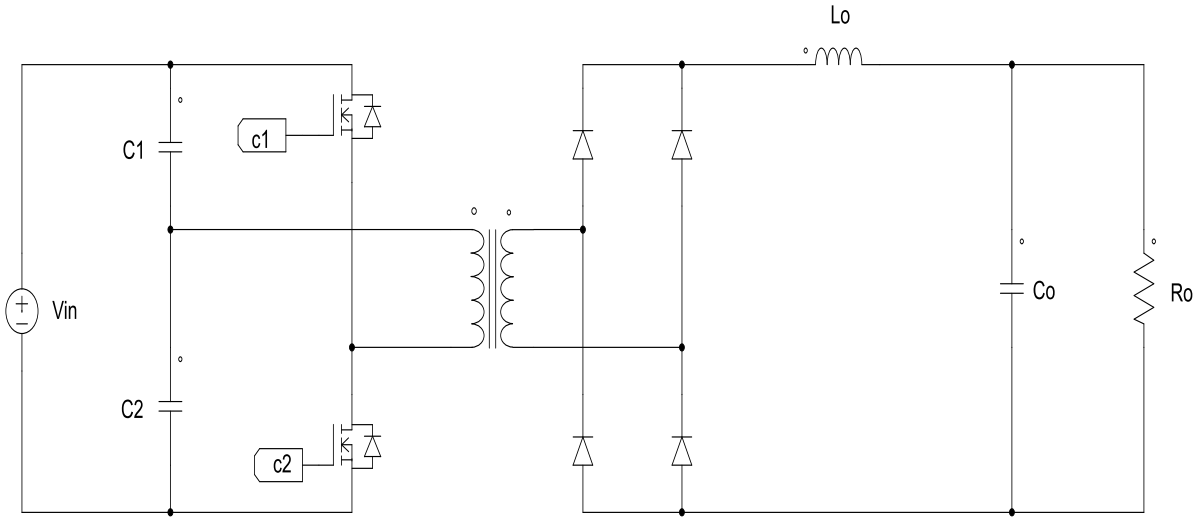

Figure 3-4: Voltage-Fed Half-Bridge Converter

3.2.1. SIMULATION SCENARIO 1

The same parameters will be utilized to compare the VFHB to the VFFB converter, but since the voltage gain is half of the VFFB, the duty cycle is double.

Table 3.3: Parameters for the First Simulation of the VFHB

Sr. No.	Parameter	Value
1.	Input Voltage (Vin)	600 V
2.	Output Voltage (Vout)	48 V
3.	Output Power (Po)	1000 W
4.	Transformer Ratio	4:1
5.	Cin	100 µF
6.	Lo	150 µF
7.	Co	22 µF
8.	C1 and C2	1 µF
9.	Switching frequency (fs)	100 kHz
10.	D	0.32

Figure 5.5 shows the results obtained from PSIM for *Table 5.3* parameters.

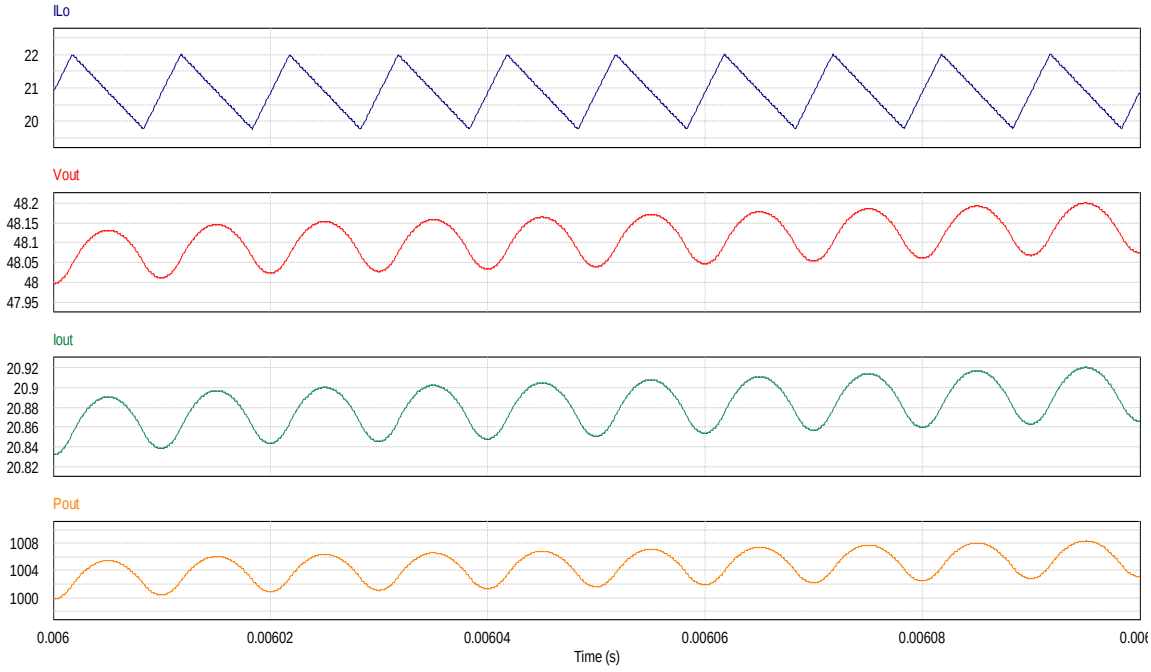

Figure 3-5: VFHB Output Waveforms for Table 5.3 Parameters

Obtaining the results from PSIM, we can notice in Figure 5.5 that the current ripple in the output inductor of the VFHB is higher than that of the VFFB. More specifically, it is twice as higher. While for the *Table-5.1* parameters the VFFB had a current oscillation in Lo of 1.10

A, the VFHB achieved 2.20 A, meaning that it requires a larger inductor to maintain the same ripple. The voltage ripple on the load was 12.52 mA.

The conduction and switching losses in steady-state for the rectifier diodes were 1.53W and 22.12W, while for the switches, these losses were 786mW and 8.8W, respectively. The rectifier topology utilized for the full-bridge to reduce the number of semiconductors resulted in increased conduction losses for the diodes.

The diodes reached switching losses close to 25W in the transient operation, higher than those in the VFFB. The conduction losses of the switches during the transient reached 2.13 W while the switching losses 13.78W.

3.2.2. SIMULATION SCENARIO 2

Similarly, to the VFFB, a second simulation is performed, reducing the frequency to 50 kHz and the input voltage to 415V. It is essential to mention that due to the reduced voltage gain of the VFHB, it was necessary to increase D.

Table 3.4: Parameters for the Second Simulation of the VFHB

Sr. No.	Parameter	Value
1.	Input Voltage (Vin)	415 V
2.	Output Voltage (Vout)	48 V
3.	Output Power (Po)	1000 W
4.	Transformer Ratio	4:1
5.	Cin	100 μF
6.	Lo	150 μF
7.	Co	22 μF
8.	C1 and C2	1 μF
9.	Switching frequency (fs)	50 kHz
10.	D	0.46

Like the VFFB converter, if the Frequency had been just decreased by half and all the other parameters were not changed, the current ripple in the output inductor would double But, in this specific case, since the input voltage was reduced. The duty cycle increased; this results in a lower ripple. Regarding the voltage ripple in the load, the value was found in the VFFB.

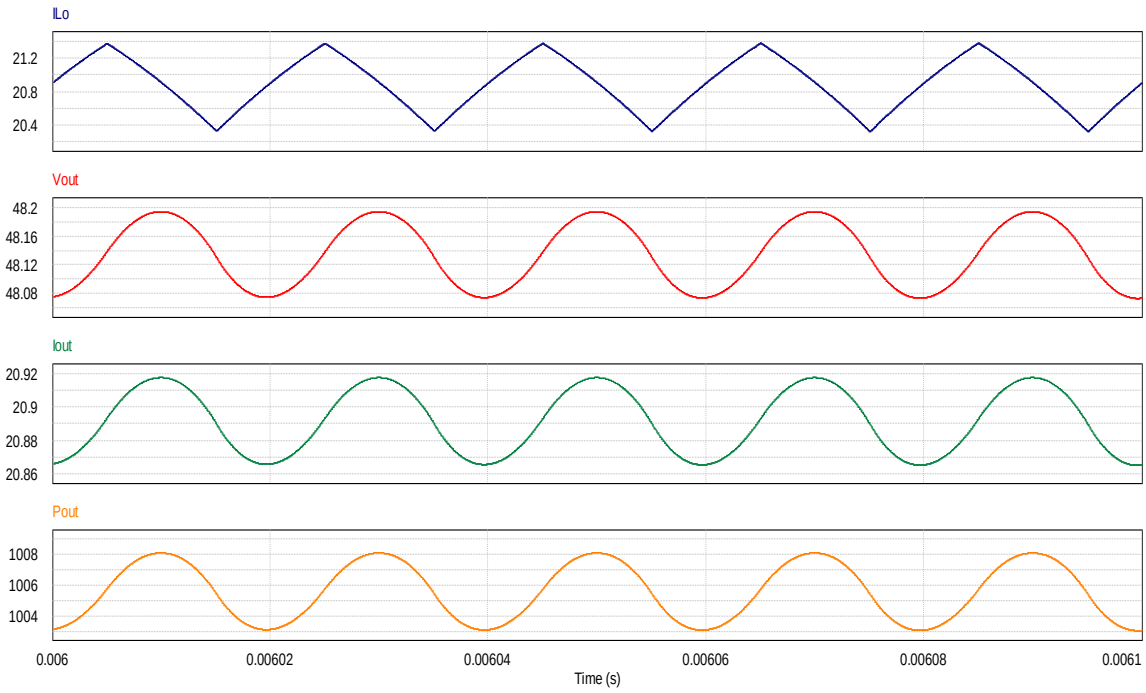

Figure 3-6: VFHB Output Waveforms for Table 5.4 Parameters

During steady-state, the conduction losses of the diodes were 708mW, and the switching losses were 19.6 W. Compared to the VFFB, the half-bridge topology presented lower losses in the rectifier diodes. However, it has more components on the low-voltage side. The switches achieved 648 mW of conduction losses and 2.99 W of switching losses during a steady state.

At the startup, the conduction and switching losses in the diodes achieved 590 mW and 24 W, respectively. The switches reached a peak loss of 3.43 W for switching and 880 mW for conduction.

3.3. CURRENT-FED FULL-BRIDGE INVERTER (CFFB)

This topology also presents a low ripple in the input current due to the reduction of the ripple provided by the delayed activation in half of the pairs of switches, besides not presenting problems related to the unbalance flow in the transformer. Among some disadvantages of this topology are a relatively high number of semiconductors, the need for bootstrap circuits for the upper switches or isolated sources, high overvoltage in the switches caused by the energy stored in the transformer leakage inductance [59] [60].

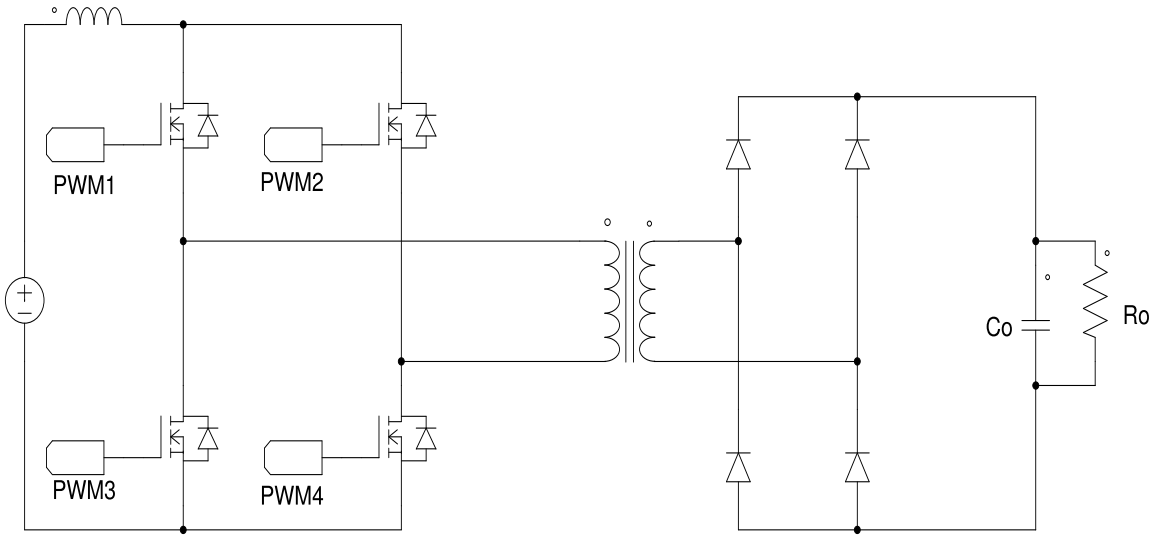

Figure 3-7: SIMULATION SCENARIO 1

Considering a photovoltaic microinverter application, the following parameters were defined.

Table 3.5: Parameters for the First Simulation of the CFFB

Sr. No.	Parameter	Value
1.	Input Voltage (Vin)	40 V
2.	Output Voltage (Vout)	400 V
3.	Output Power (Po)	400 W
4.	Transformer Ratio	1:6
5.	L1 and L2	150 µF
6.	Co	470 nF
7.	Switching frequency (fs)	100 kHz
8.	D ideal	0.7
9.	D used	0.707

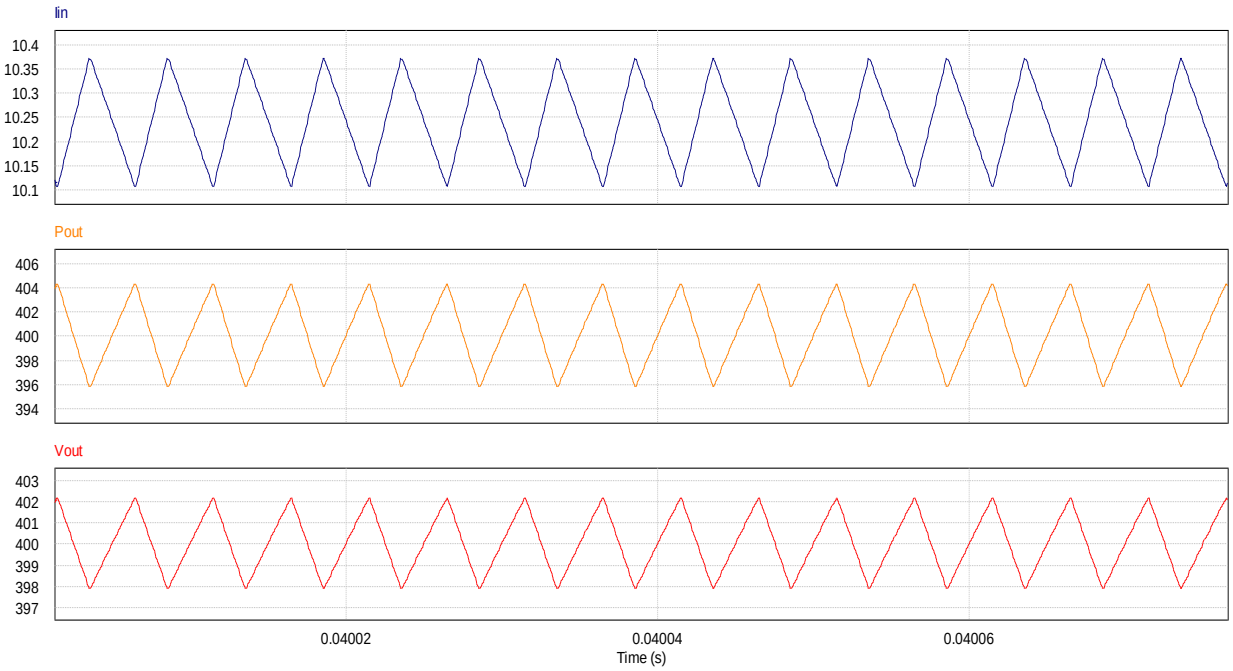

Figure 3-8: CFFB Waveforms for Table 5.5 Parameters

Unlike the CFHB converter, the CFFB has only one input inductor, which processes the total power of the converter. Therefore, this inductor is bulky. The voltages and current oscillations in the output are the same as the CFHB converter.

The steady-state power losses on the diodes were 1.95 W and 470 mW due to conduction and switching, respectively. At the same time, the switches released 1 W by switching and 1.88 W by conduction.

At the startup, the transient switching losses of the switch reached a peak equal to 3.15 W, and the conduction losses got a maximum value of 6.03 W. The peak conduction losses reached 2.13 W for the diodes, and the switching losses' maximum value was 948 mW.

3.3.1. SIMULATION SCENARIO 2

Like in the CFHB simulation, a second simulation has been performed, reducing switching frequency and voltage.

Table 3.6: Parameters for the Second Simulation of the CFFB

Sr. No.	Parameter	Value
1.	Input Voltage (Vin)	20 V

2.	Output Voltage (Vout)	400 V
3.	Output Power (Po)	400 W
4.	Transformer Ratio	1:6
5.	L1 and L2	150 µF
6.	Co	470 nF
7.	Switching frequency (fs)	50 kHz
8.	D ideal	0.85
9.	D used	0.861

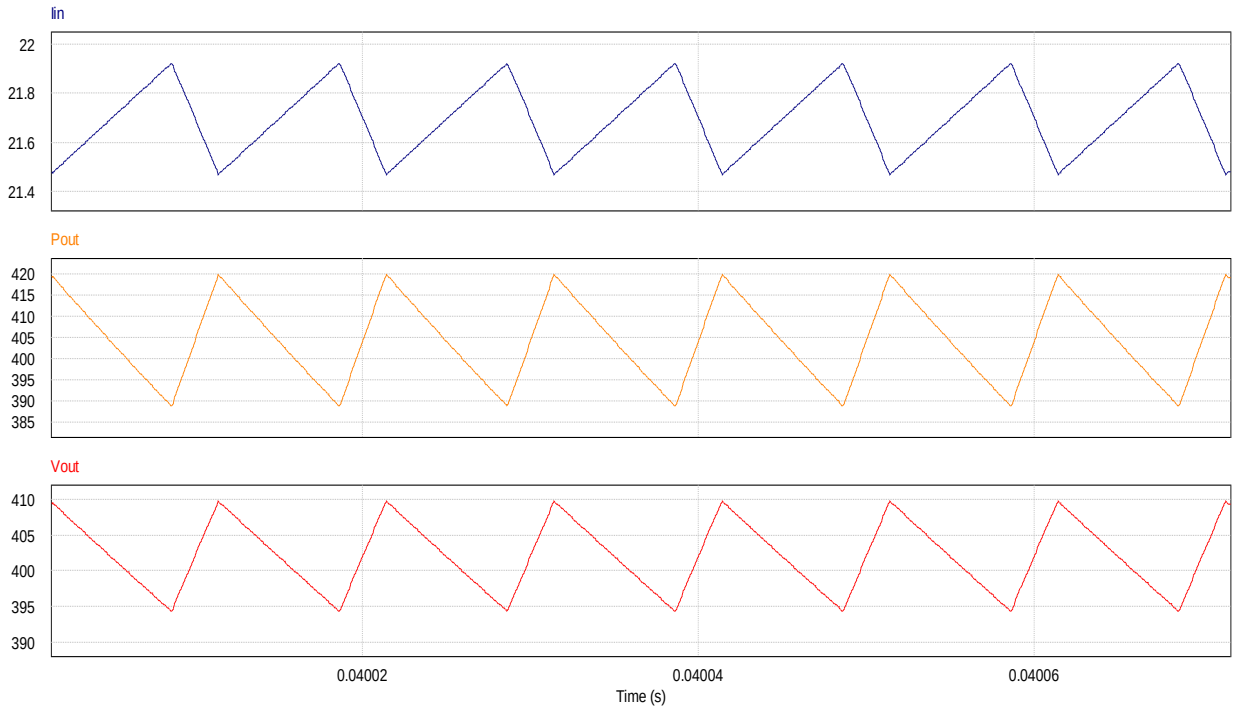

Figure 3-9: CFFB Waveforms for Table 5.6 Parameters

Like the other converter, a decrease in frequency implies a higher current ripple in the inductor, although the input current increased due to a low voltage.

The conduction and switching losses in the diodes during the steady-state operation were 1.67 W and 604 mW, respectively. While in the transient startup, they reached 1.76 W and 678 mW.

The switches released 7.19 W of conduction losses and 3.62 W of switching losses at a steady state. But, at the startup, the peak switching losses were 4.26 W, and the maximum conduction losses were 8.43 W.

3.4. CURRENT-FED HALF-BRIDGE INVERTER (CFHB)

Compared to the CFFB converter, the input inductor is replaced by two inductors. The number of semiconductor switches is reduced by half, resulting in lower implementation cost and

volume, and does not demand isolated sources or circuits for bootstrap. In addition, the inductances of L1 and L2 are equal. Therefore, the current in these elements is equal to half the input current, having two inductors of less volume instead of a single more voluminous inductor, as in the case of the converter full-bridge. The switches are activated with the same cyclic ratio (greater than 0.5) with a phase-shift of half the switching period between them, which reduces the ripple in the input current [61].

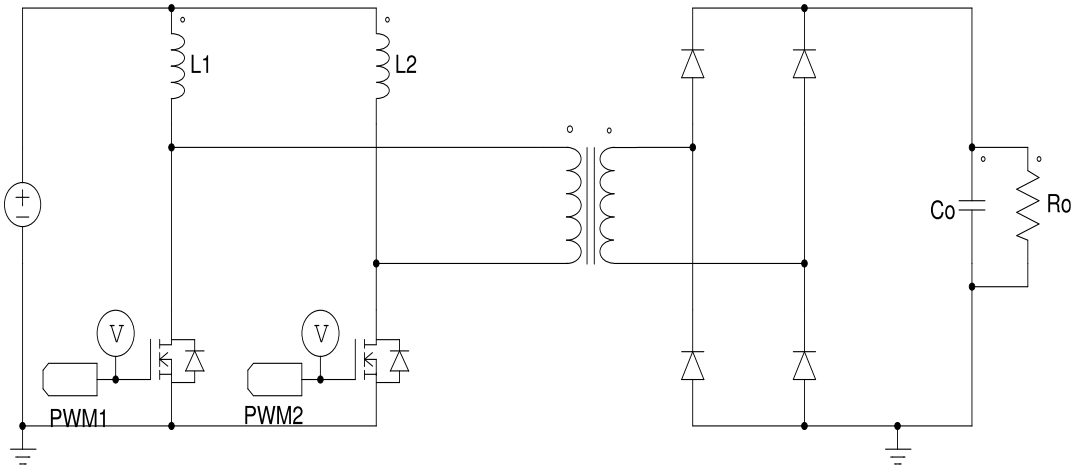

Figure 3-10: Current-Fed Half-Bridge Converter

3.4.1. SIMULATION SCENARIO 1

Like the CFFHB and considering a photovoltaic microinverter application, the following parameters were defined.

Table 3.7: Parameters for the First Simulation of the CFHB

Sr. No.	Parameter	Value
1.	Input Voltage (Vin)	40 V
2.	Output Voltage (Vout)	400 V
3.	Output Power (Po)	400 W
4.	Transformer Ratio	1:3
5.	Lin	300 µF
6.	Co	470 nF
7.	Switching frequency (fs)	100 kHz
8.	D ideal	0.7
9.	D used	0.705

Considering these parameters, the current ripple in the inductors was 1.8A, and the input current oscillation was half of it, which is a great advantage of this converter. The output voltage ripple was 4.27 V.

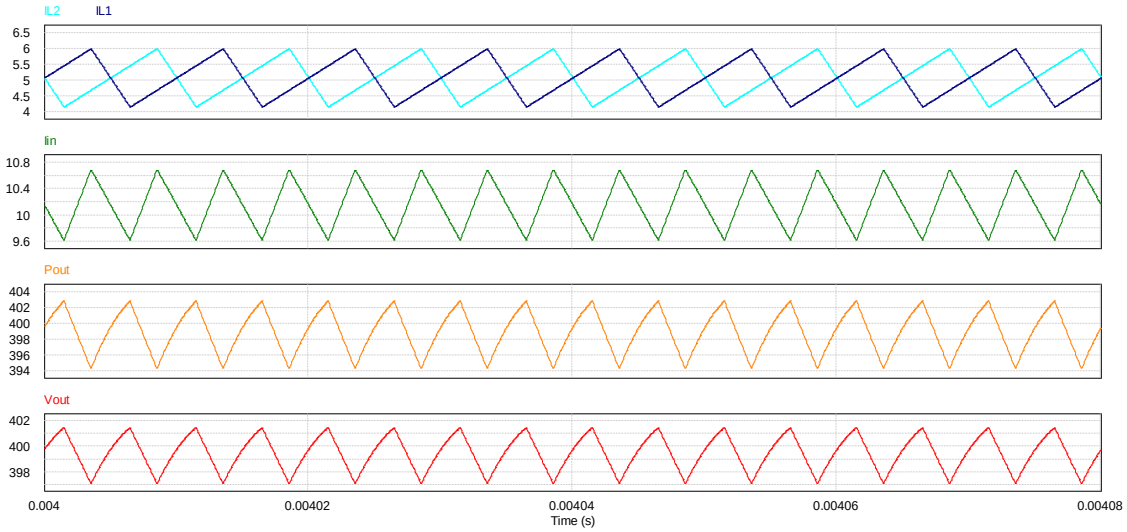

Figure 3-11: Waveforms of the CFHB Converter for the Parameters Presented in Table 5.7

At the startup, the power losses in the switches reached 2.46 W, while the conduction losses peak was 20.20 W due to the high current peak. The transient switching losses reached 3.37 W for the diodes, and the conduction losses are 1.8 W.

During steady-state operation, the losses in the diodes were 857 mW for switching and 403 mW for conduction. The switching and conduction losses were 475 mW and 1.87 W for the switches.

3.4.2. SIMULATION SCENARIO 2

The second simulation's parameters are established by reducing the frequency and input voltage.

Table 3.8: Parameters for the Second Simulation of the CFHB Converter

Sr. No.	Parameter	Value
1.	Input Voltage (Vin)	20 V
2.	Output Voltage (Vout)	400 V
3.	Output Power (Po)	400 W
4.	Transformer Ratio	1:3
5.	Lin	300 µF
6.	Co	470 nF
7.	Switching frequency (fs)	50 kHz
8.	D ideal	0.85

9.	D used	0.855

One can notice from the figure below a significant impact of the frequency reduction on the output voltage ripple, which had 14.23 V of oscillation. The current in the inductors gets the same effect.

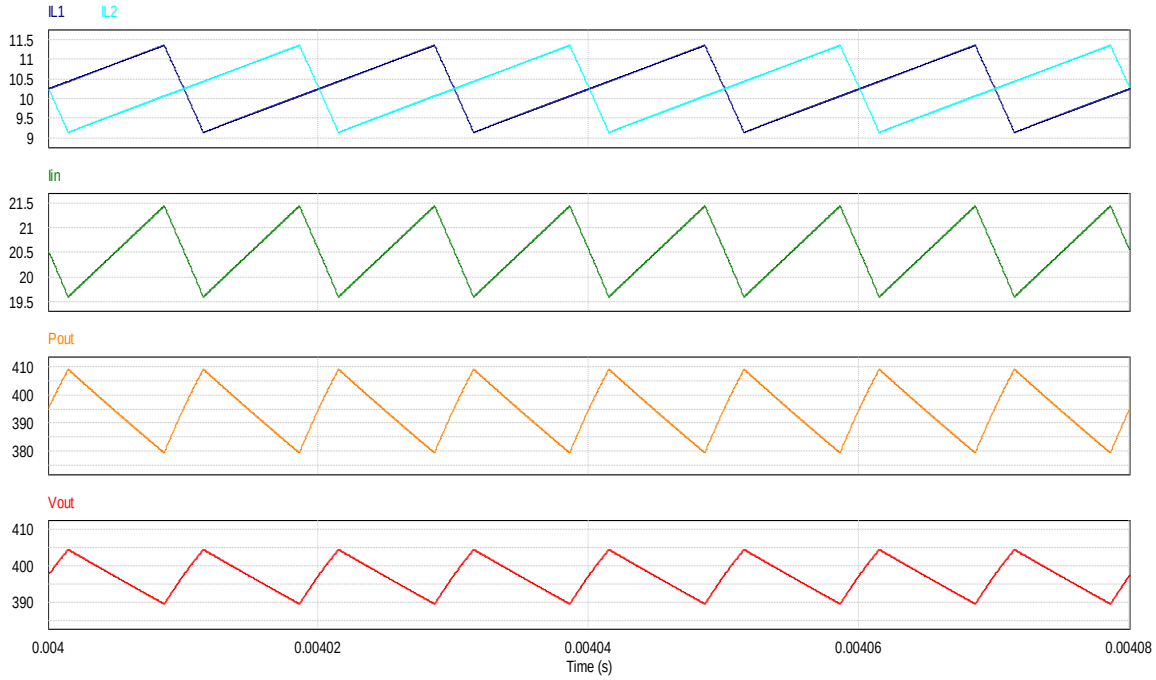

Figure 3-12: Waveforms of the Second Simulation of the CFHB Converter

The steady-state power losses of the diodes for the parameters of *Table 5.8* were 895mW for conduction and 1.03 W for switching, higher than in the first scenario. The switches released 802.7 mW of switching losses and 6.41 W of conduction losses. This increase is due to the current increase as an outcome of the input voltage reduction and a higher duty cycle.

During the startup, the peak conduction losses and switching losses for the switches were 19.78 W and 1.85 W, while in the diodes, these values reached 1.85 W and 1.94 W, lower than in the first scenario.

Voltage-fed converters are widely used in step-down applications such as switch-mode power supplies, battery chargers, UPS, etc. From the simulations, it was possible to notice that the voltage gain of the VFFB is double that of the VFHB, and the losses on the semiconductors of the half-bridge topology were higher. Moreover, in practical applications, since the input voltage is divided between the capacitors C1 and C2, the half-bridge converter suffers from limitations at higher power levels. But the voltage-fed half-bridge converter has the advantage

of utilizing just half of the switches of the full-bridge topology, making it a more straightforward converter to operate.

The half and full-bridge topologies were simulated considering PV applications in the current-fed converters. The CFFB topology has a higher number of semiconductors, requires bootstrap circuits for the upper switches or isolated sources, and has a bulky inductor, raising implementation costs and volume. Regarding losses, the simulation results showed higher losses for the CFFB converter, and the use of SiC switched provided reduced switching losses, even at high frequencies.

Finally, although decreasing the switching frequency could reduce losses and, as a result, increase the voltage/current variations, the decrease of the input voltage raised the current levels, also implying higher losses for both converters.

4. DESIGNING OF THREE PHASE INVERTER

The final objective of my thesis was to design a three-phase CSI. The design and results are shown in this chapter.

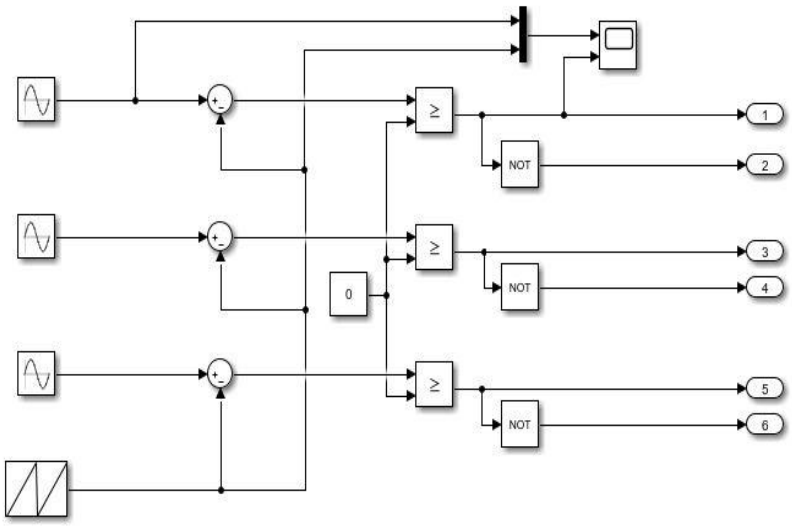

Figure 4-1: PWM Generator

This generator shown in figure 4.1 is used to create the switching gate pulses for the MOSFETSs. A sawtooth wave is compared with three Sine wave sources to create the required pulses at 120-degree phase shift. The resulted wave is shown in the figure 4.2 with upper figure showing the comparison between phase one and triangular wave, and the lower graph showing the resulted pulses for MOSFETS 1.

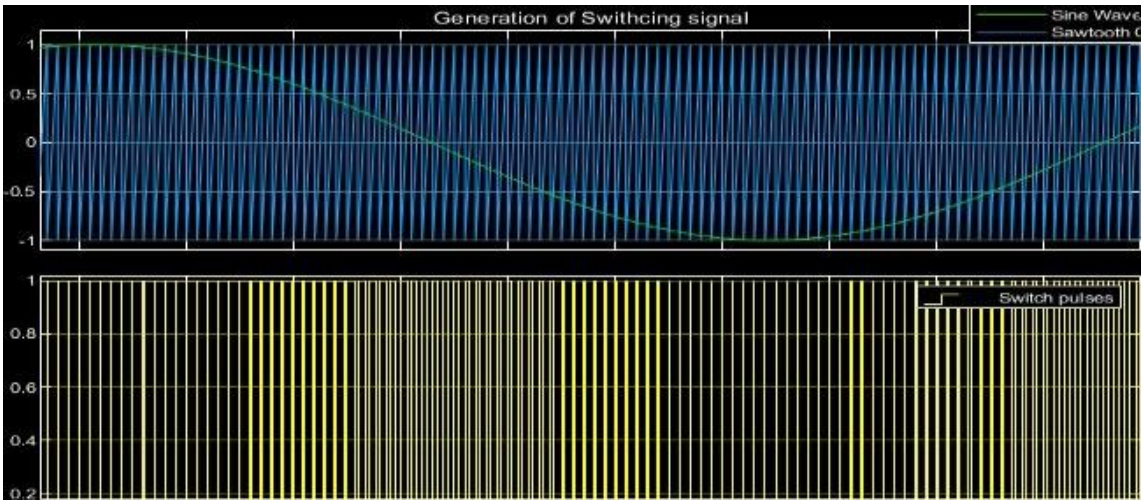

Figure 4-2: PWM generated for MOSFET switches

The figure 4.3 shows the whole system with three phase star connected inverter with R-L load and six MOSFETSs. An Ac current source is used as an input to the circuit. The gains are used to create RMS values of voltages and current from peak values of all phases. The input current is 50 Amperes and the resistor and inductor load per phase is 15 ohms and 0.006 Henry. The circuit has been tested with two frequencies of 5kHz and 10kHz and the result are show in the following figures.

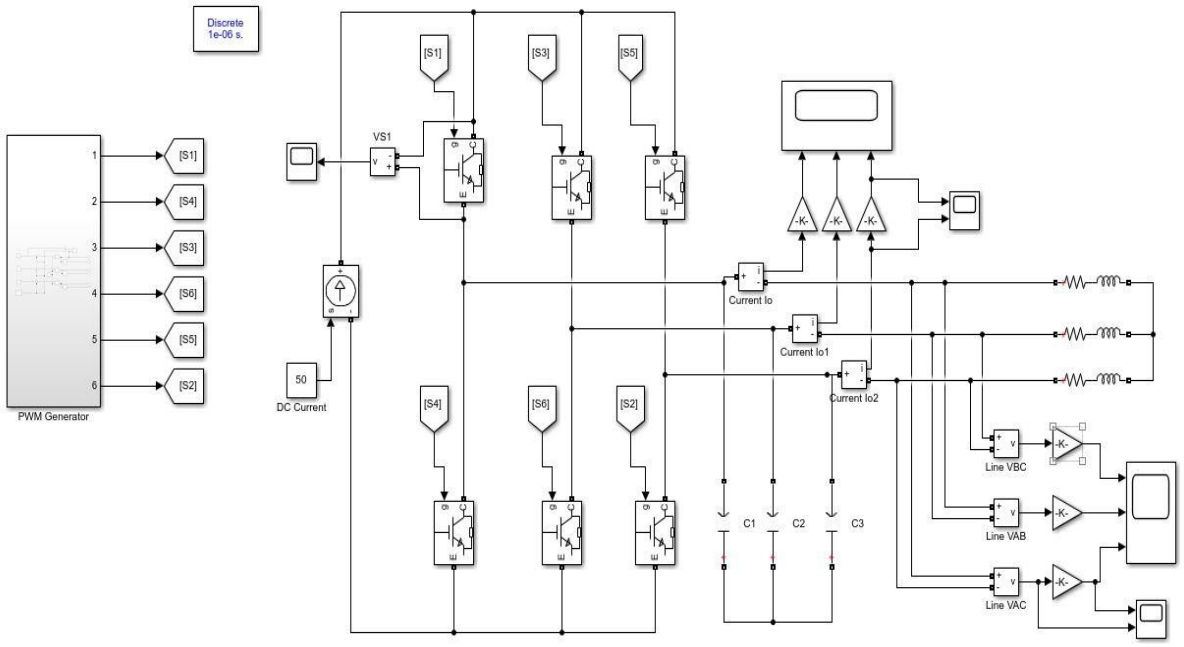

Figure 4-3: Three phase CSI Simulation

Fig 4.4 shows the RMS currents graphs at 5 KHz frequency for all the three phases A,B and C. The RMS current has peak value of 23 Amperes.

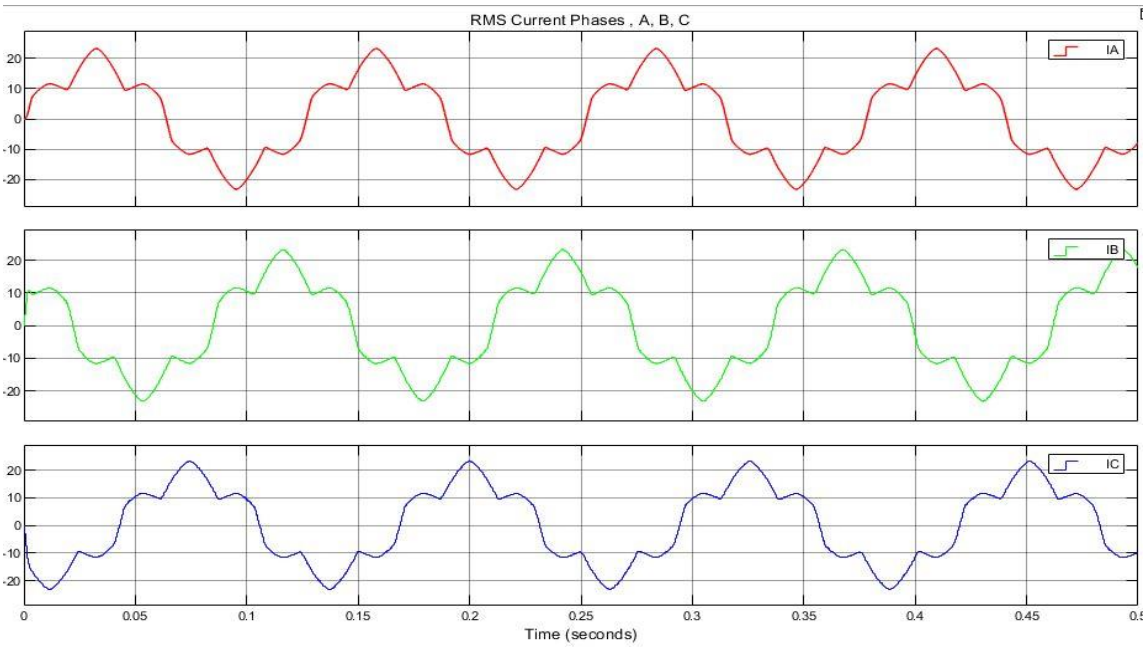

Figure 4-4: RMS Currents Phase A, B, C

Fig 4.5 shows the comparison between RMS to Peak Voltages with maximum RMS value of 544 Volts and Peak to Peak voltages of 769 Volts at frequency 5kHz.

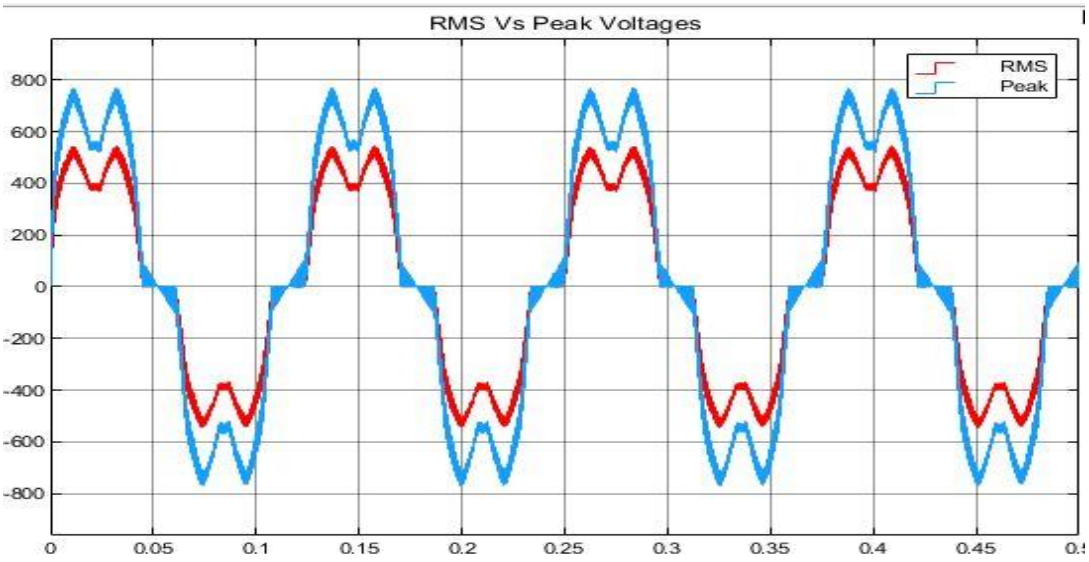

Figure 4.5: Comparison between RMS to Peak Voltages

Fig 4.6 shows the comparison between RMS to Peak Currents with maximum RMS value of 23A & Peak to Peak Current of 32.7 A at frequency 5kHz.

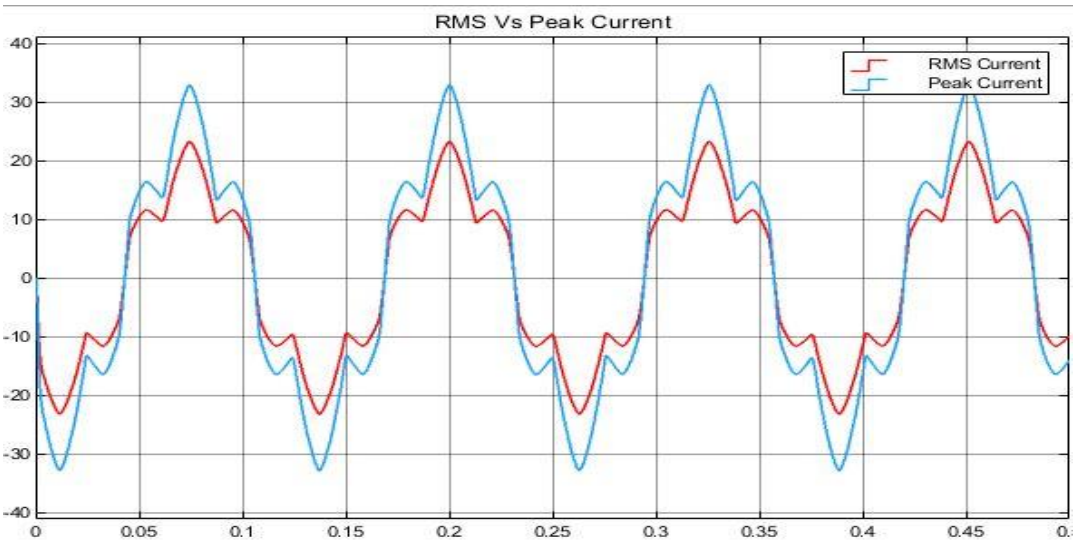

Figure 4.6: RMS Vs Peak Current

Figure 4.7 shows the results at 10 Khz frequency for RMS Currents of all three phases A, B, C with the maximum value of 23A

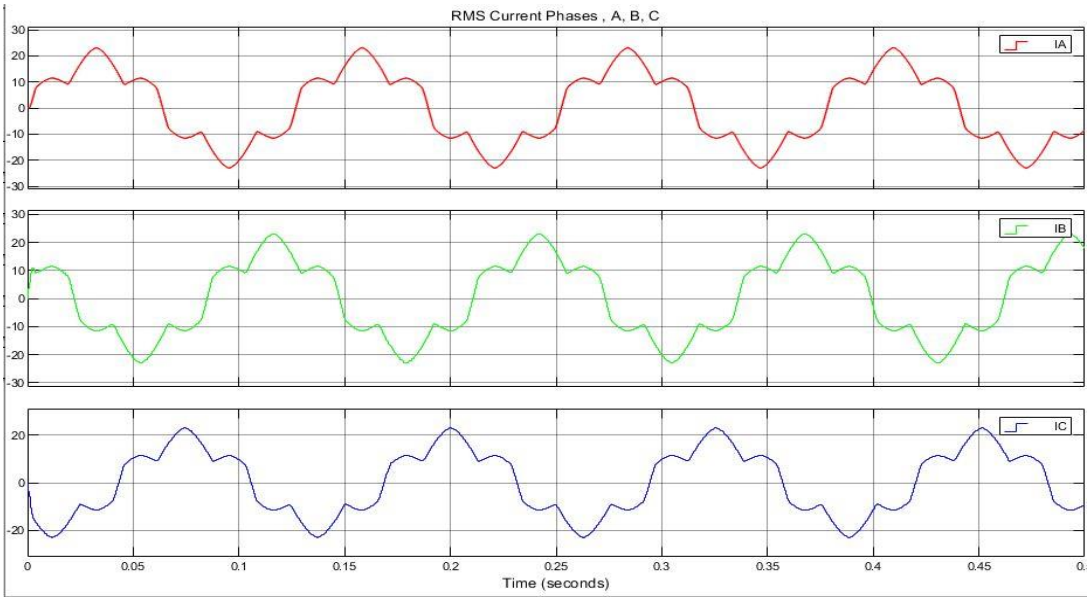

Figure 4.7: RMS Current phases A, B, C at 10kHz

Fig 4.8 shows the comparison between RMS and Peak Current at 10kHz, the RMS maximum value is 23 A and Peak to Peak value is 32.7 A.

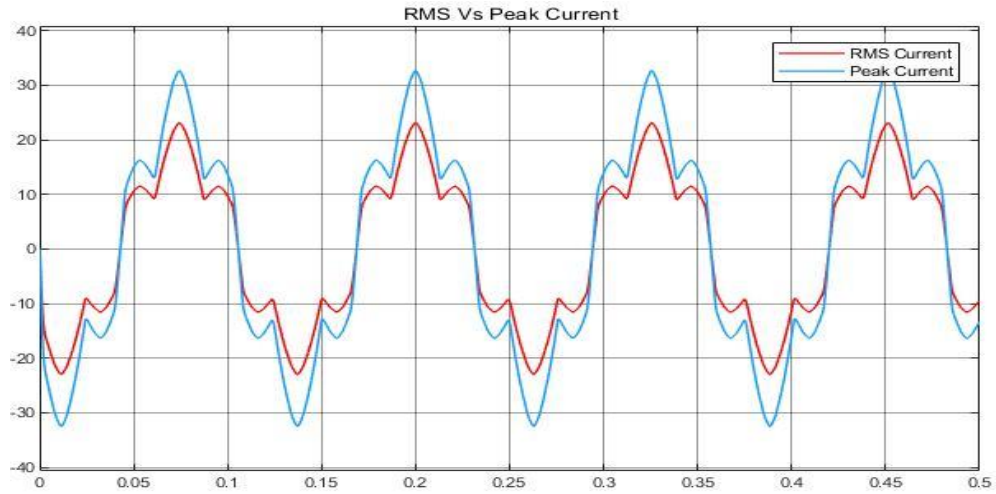

Figure 4.8: RMS Vs Peak Current

Fig 4.9 shows the comparison between RMS to Peak voltages at 10 Khz, with maximum RMS value 531 Volts and Peak to Peak value 750 Volts.

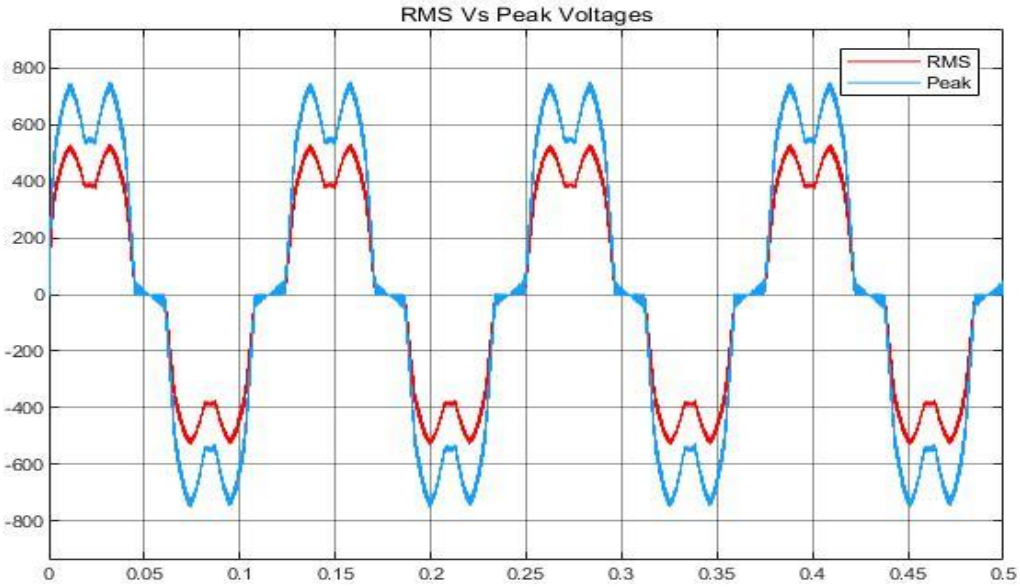

Figure 4.9: RMS Vs Peak Voltages

Table 4.1: Shows the input and output parameters for the three-phase CSI

	5KHz	10Khz
RMS Voltage	544 Volts	531 Volts
RMS Current	23 A	23 A
Peak Voltage	769 Volts	750 Volts
Peak Current	32.7 A	32.7 A

The figures show promising results for the three phase inverter simulations. The simulation is working perfectly and giving the desired results for all the currents and voltages, working smoothly on different higher frequencies.

5. CIRCUIT CONFIGURATION FOR PCBs

This part of the thesis deals with theoretical background for a general half-bridge, full-bridge, and three-phase CSIs configuration using SiC switches. The general circuits show the basic configuration of SiC switches in common source mode to obtain reverse voltage blocking for above mentioned circuits.

For the CSI to work appropriately, the switches must have both the reverse voltage blocking (RB) and bidirectional conduction mode. Sic switches have this unique property that in some combinational cases, they can be used in pairs to act as both bidirectional switches and have reverse voltage blocking capability with significantly fewer losses in both forward and reverse conduction because of the symmetrical on state V-I characteristics for both forward and reverse conduction [62]. Common source and common drain combination in SiC switches reduce the losses compared to using a freewheeling diode.

The *Figure 5.1* shows the combinations with IGBT with diodes, *the* common source combination of SiC switches and common drain mode with SiC switches [62].

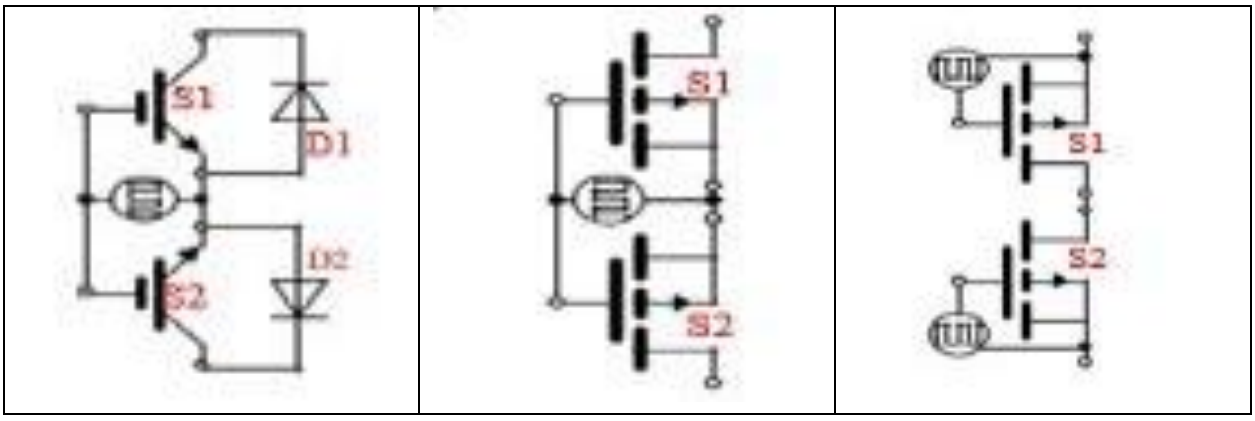

Figure 5-1 [Left to right]: IGBT with Diodes, Common Source SiC, and Common Drain SiC configuration

The common source has an advantage of a simple design gate drive circuit because a single gate drive can be used for both the switches. In contrast, the standard drain has lower resistances but uses separate gate drivers for each switch.

5.1.1. HALF BRIDGE

A half-bridge is a DC – AC converter that primarily uses two switches to control the output voltage. The load current in a half-bridge circuit flows in both direction because of which it is also known as a two-quadrant converter. *Figure-4.2* below shows a general circuit diagram of a half-bridge CSI (CSI) using four SiC switches in common source mode.

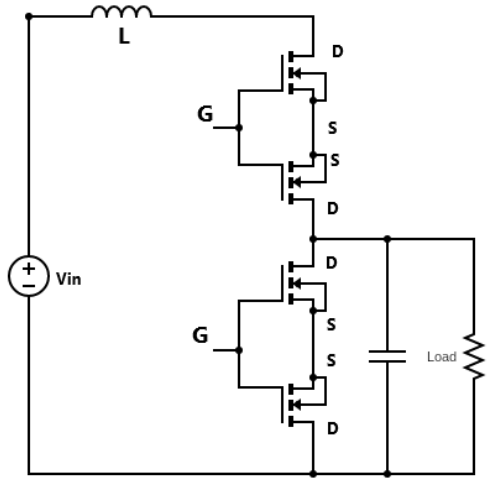

Figure 5-2: Circuit Diagram of Half-Bridge CSI

5.1.2. FULL BRIDGE

A full-bridge inverter requires eight SiC switches in four pairs. *Figure-4.3* shows a full-bridge inverter circuit diagram in common source mode.

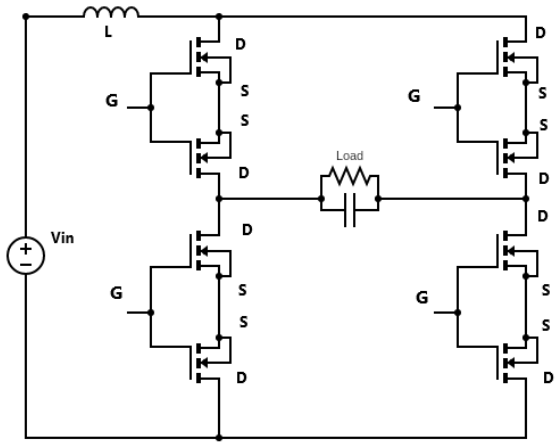

Figure 5-3: Circuit Diagram of a Full Bridge Inverter

5.1.3. THREE-PHASE INVERTERS

A three-phase inverter is used to convert DC voltage to a three-phase AC supply with the help of switches and drivers. A three-phase inverter is mainly used for high power applications and HVDC power transmission.

In a basic three-phase CSI, we are using twelve SiC switches. There are three arms in the circuit of a three-phase inverter. Generally, all the arms are delayed by 120 degrees each

to generate a three-phase AC supply. A general circuit diagram of a three-phase CSI using SiC switches is shown below.

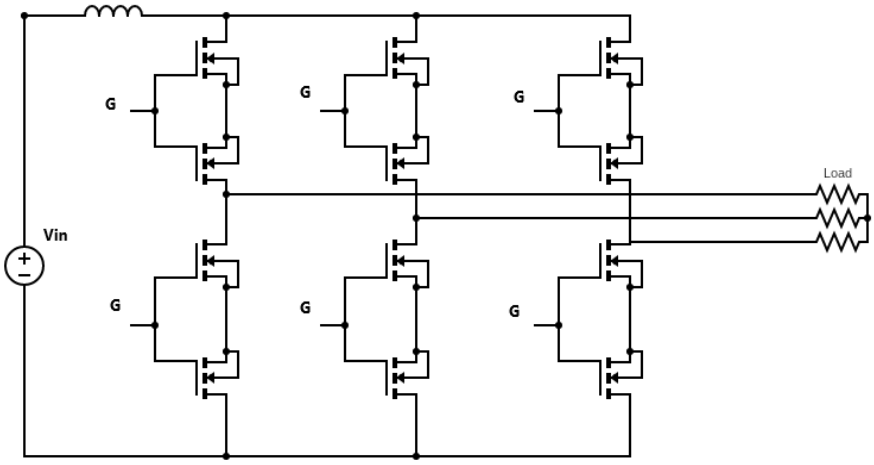

Figure 5-4: Three-Phase CSI Circuit Diagram

Such an inverter is used chiefly in variable frequency drive applications, HVDC transmission, and UPS circuits.

5.1.4. SICs

SiC switches are preferred in many applications. It is due to their following traits.

- High blocking voltages due to the wider bandgap
- Lower ON state resistance
- Higher thermal conductivity

Some of the drawbacks of using SiC MOSFETs are given below.

- Need of Gate Drives
- High cost as compared to Si MOSFETs

To get better performance, these drawbacks are often neglected. Generally, the results are worth the trouble.

6. PARTS DESIGNING AND CONSIDERATIONS

This section includes the circuit designing, considerations, and simulation results of all three parts involving SiC. These are half-bridge, full-bridge, and three-phase inverter. There PCB is also designed and presented in this section. The Simulations are designed in LTspice software to test the general condition for the design of PCBs in easy EDA software. That's why the detailed information for the circuit in these simulations isn't discussed in detail.

LTspice software is a high-performance SPICE simulation software, schematic capture, and waveform viewer with enhancements and models for easing the simulation of analog circuits. Its libraries provide a wide range of macro models for most Analog Devices switching regulators, amplifiers, as well as a library of devices for general circuit simulation.

The enhancements to SPICE have made simulating switching regulators extremely fast compared to standard SPICE simulators, allowing the user to view waveforms for most switching regulators in just a few minutes [63].

While LTspice has made it easier for us to draw schematics and simulate circuits with accurate results, **Easy EDA** has made it even simpler to make a schematic PCB. It is a more accessible and powerful online PCB design tool. More than 1 million real-time updated components have been created, letting the user focus on designing and building or importing their own shared libraries [64].

6.1. HALF BRIDGE

The half-bridge CSI circuit that is to be designed and fabricated includes some basic steps that involve the circuit creation in LTspice. Its simulation, and then the PCB designing while getting the accurate results. Thus, all these steps are presented as follows. The designing software is used in LTspice, whereas Easy EDA is used for PCB designing.

6.1.1. LTSPICE SCHEMATICS

The half-bridge circuit is constructed in LTspice software and is presented in the following figure.

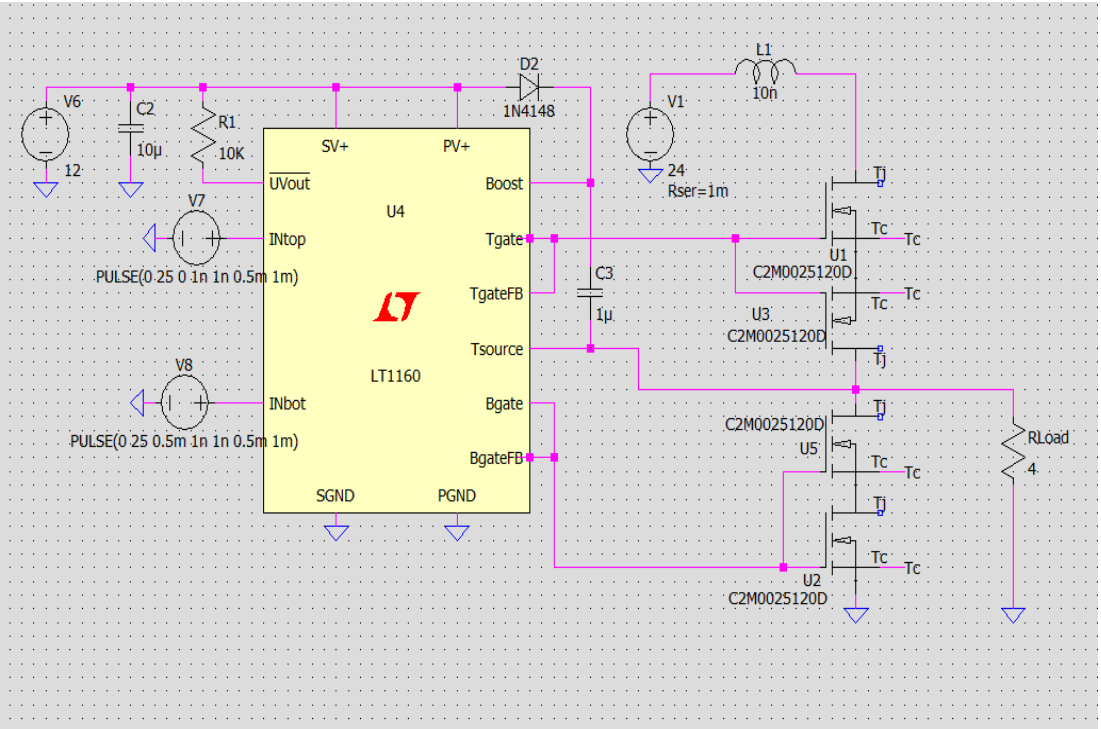

Figure 6-1: LTspice Schematics of Half-Bridge Circuit

6.1.2. SIMULATION RESULTS

The circuit diagram of the half-bridge that is designed in LTspice (as shown in *Figure 4.1*) is simulated for its input and output. The following figures show the input and output graphs as the simulated results. The input voltage was 25V DC.

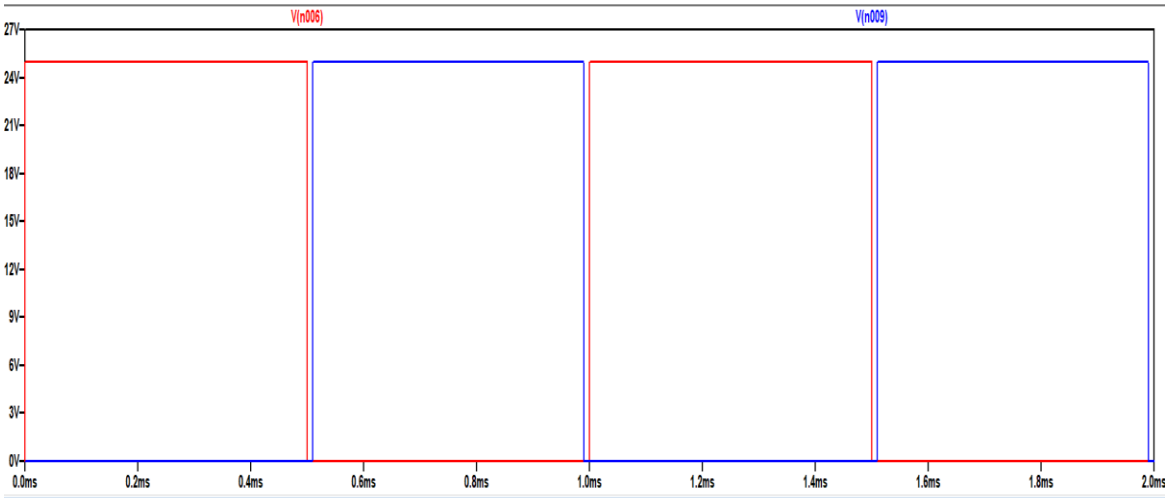

Figure 6-2: Input Given to the Half-Bridge

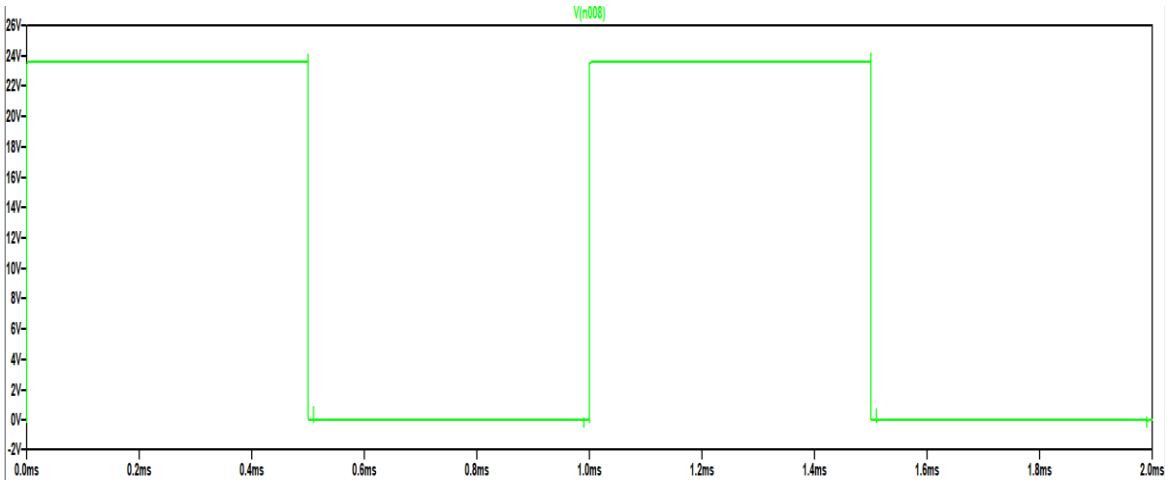

Figure 6-3: Output Obtained from the Half-Bridge

6.1.3. PCB DESIGN

For the fabrication and assembly of the project's hardware, the PCB of the circuit is designed. As the results obtained are precisely what is required, the circuit is working accurately and can be transformed into hardware. Thus, the following figure shows the designed PCB for the half-bridge CSI circuit. The PCB design is made using the Easy EDA tool of MATLAB that is the best tool for clean and accurate PCB designing and wiring.

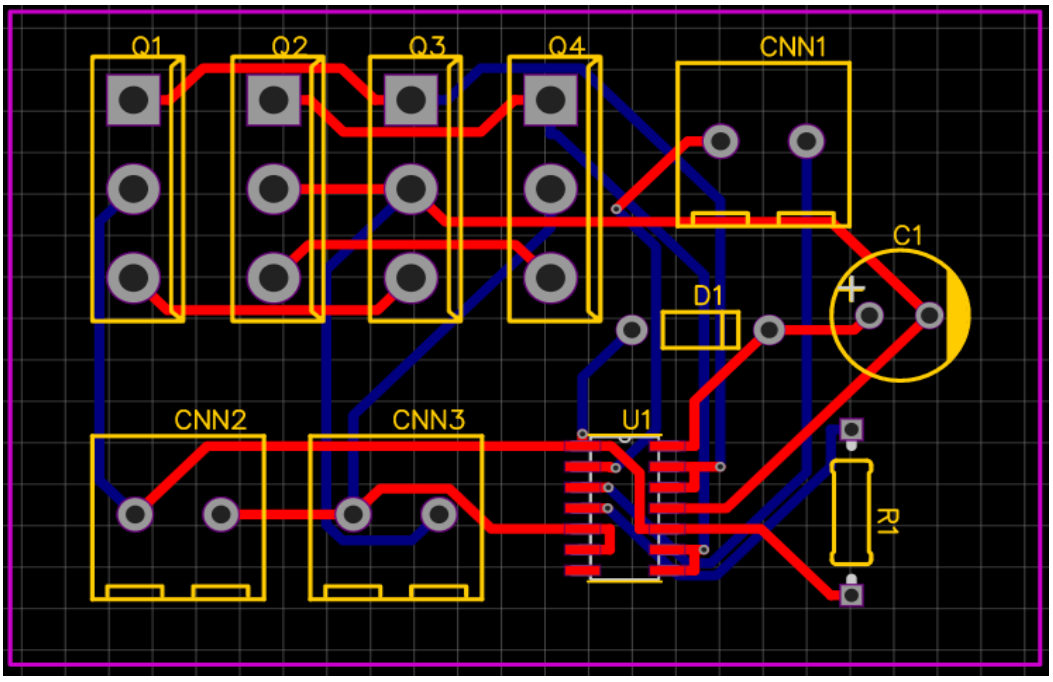

Figure 6-4: PCB Design Made Using Easy EDA

6.2. FULL BRIDGE

The full-bridge CSI involving SiC switches is also designed in LTspice software. It is then simulated to check the working of the circuit. After getting the desired results, the constructed

circuit is transformed into PCB design using Easy EDA – a MATLAB tool best known for PCB designing and wiring. All these performed steps are presented as follows:

6.2.1. LTSPICE SCHEMATICS

Like the half-bridge circuit, the full-bridge circuit is designed in the LTspice schematics and displayed in the following figure.

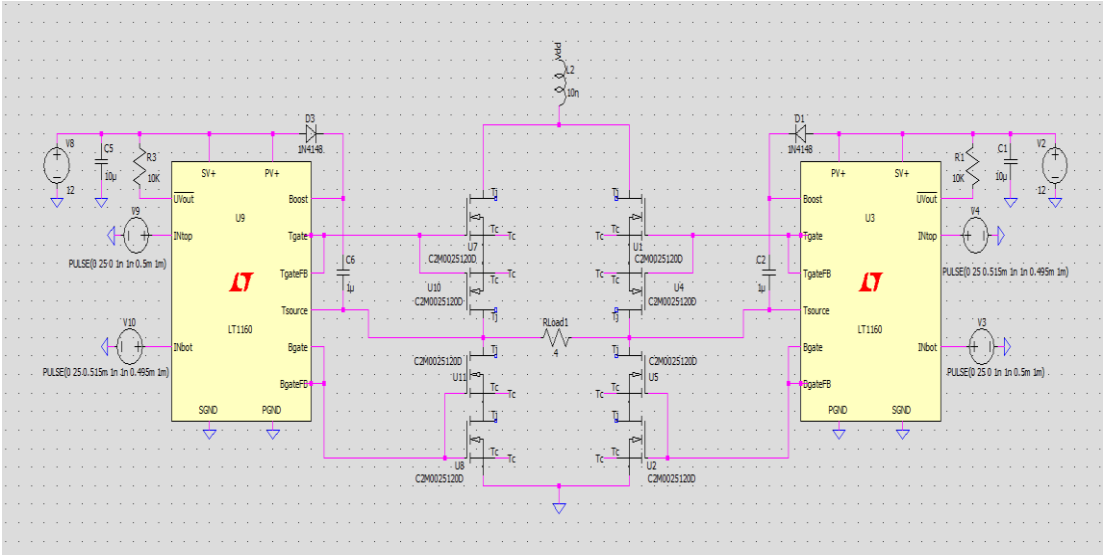

Figure 6-5: LTspice Schematics of Full-Bridge Circuit

6.2.2. SIMULATION RESULTS

The circuit designed in LTspice schematics is simulated to verify the accuracy and stability of the output. Thus, the simulation results that are achieved are shown in the following figure.The input voltage used in this simulation was 25V DC.

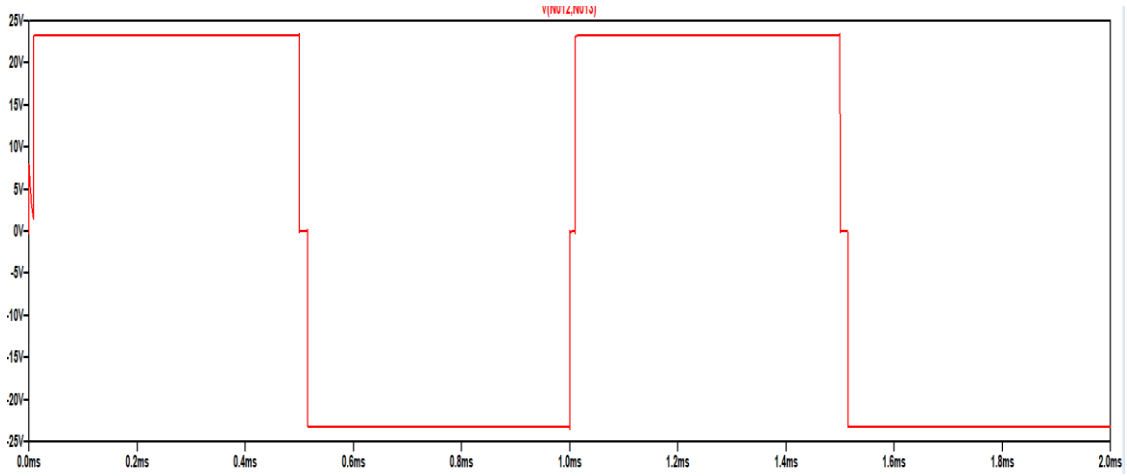

Figure 6-6: Output Obtained from the Full Bridge Circuit

6.2.3. PCB DESIGN

As the results obtained are accurate and precisely what we have expected. Thus, this means the full-bridge circuit is working accurately, and it can be transformed into hardware. Thus, the PCB of the circuit is designed using the Easy EDA software, and the following PCB is designed.

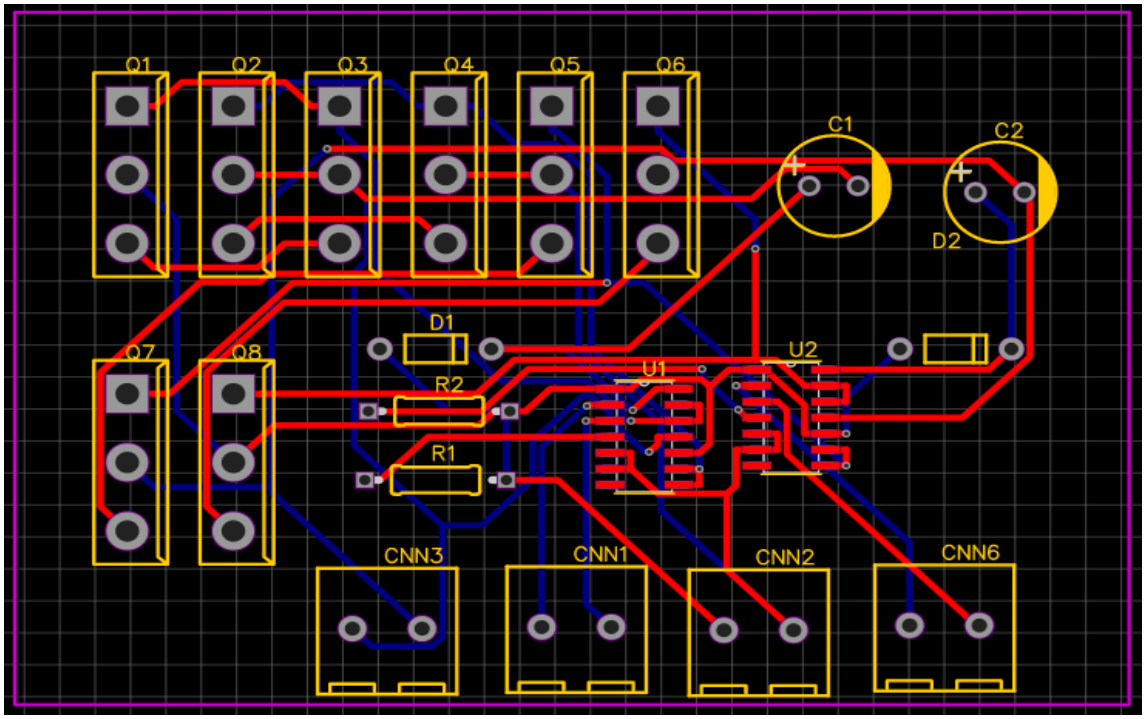

Figure 6-7: PCB Design Made Using Easy EDA

6.3. THREE-PHASE INVERTERS

Like the half-bridge and full-bridge circuits, the three-phase inverter circuit is designed and simulated on LTspice. The circuit seems to work efficiently. Thus, its PCB is designed and displayed along with circuit and simulation results in the following sections.

6.3.1. LTSPICS SCHEMATICS

The three-phase inverter is designed and constructed in LTspice schematics, and it is shown in the following figure.

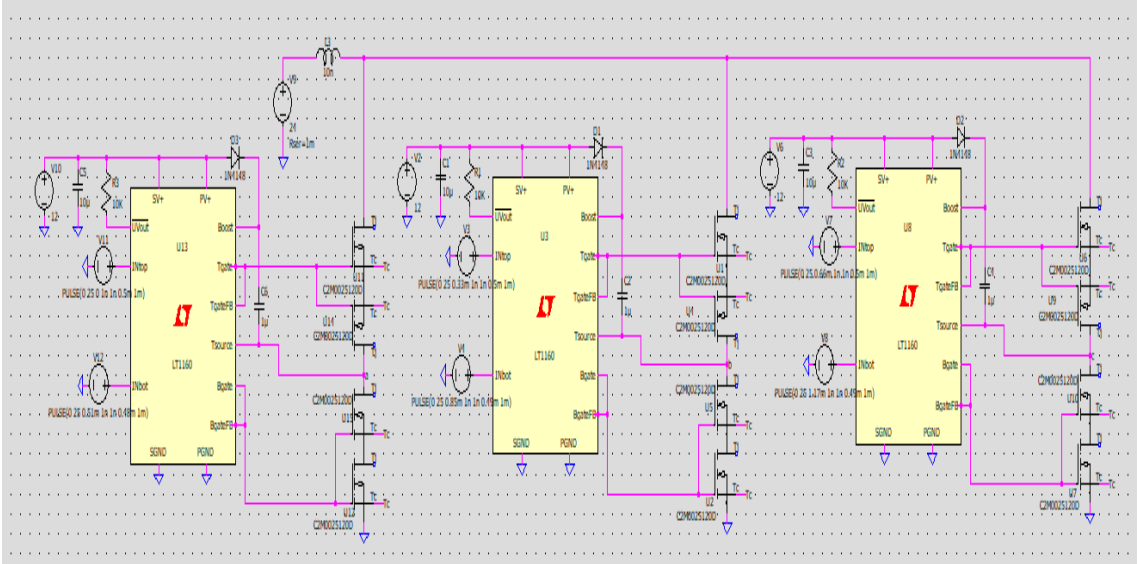

Figure 6-8: LTspice Schematics of Three-Phase Inverter Circuit

6.3.2. SIMULATION RESULTS

The three-phase inverter circuit shown in *Figure 4.8* is simulated, and the following results are obtained. The input voltage used in this simulation was 25V DC.

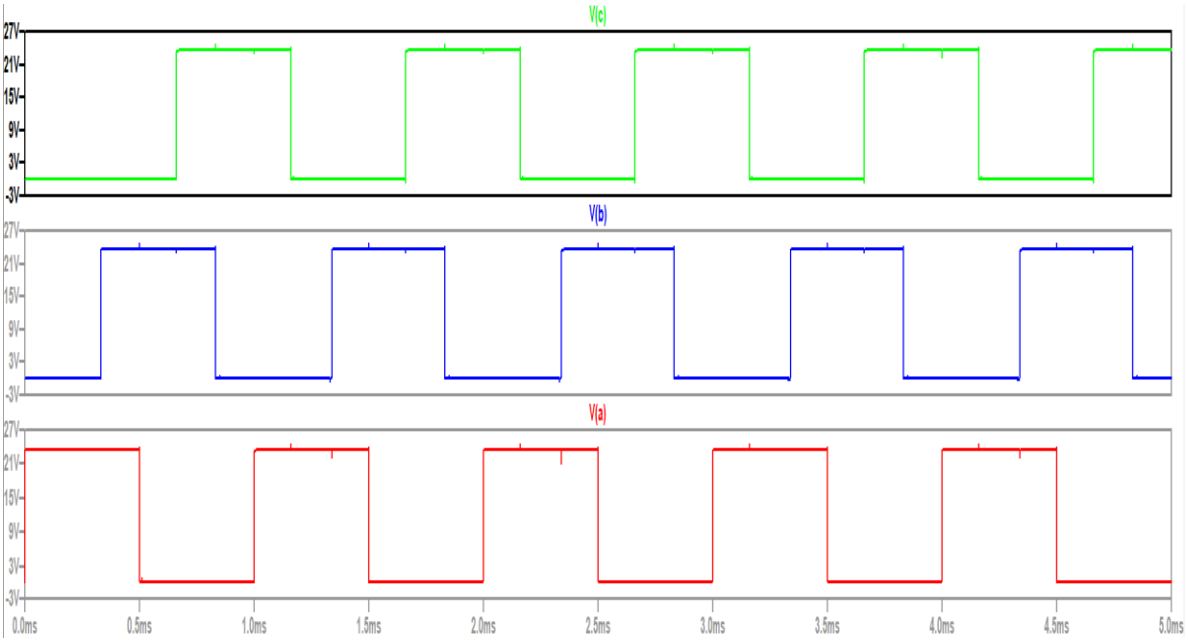

Figure 6-9: Output Obtained from the Three-Phase Inverter

6.3.3. PCB DESIGN

Based on the above results that seemed accurate, the PCB of the circuit is designed using the Easy EDA tool of MATLAB. The designed PCB is shown in the following figure.

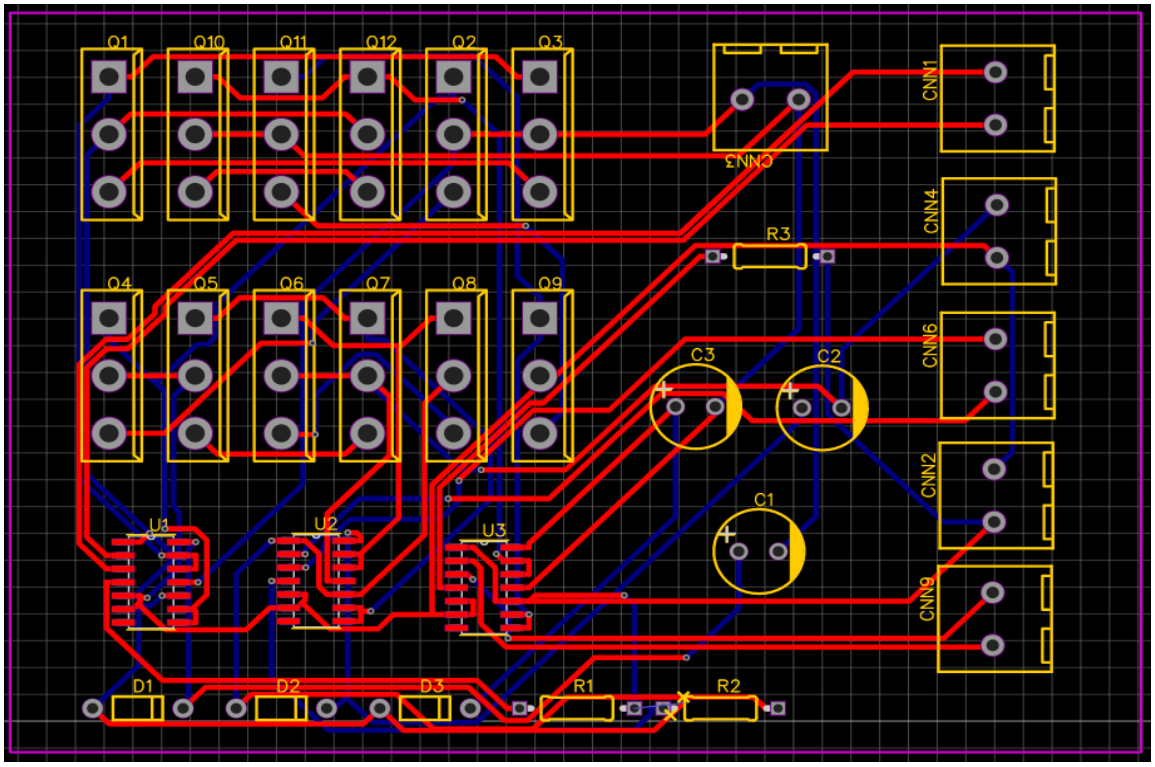

Figure 6-10: PCB Design Made Using Easy EDA

7. HARDWARE TESTING

7.1. SiC MOSFETS (C3M0040120K)

In this part, we are obtaining an additional objective for this thesis by doing some simple hardware experiments to test Cree's N-channel 3rd generation SiC MOSFETS (C3M0040120K) with its comparative gate driver Cree's CGD15SG00D2, both shown in figure 7.1 with their connections and characteristics. These devices can be used in future to implement and test all the circuits simulated and discussed in this thesis.

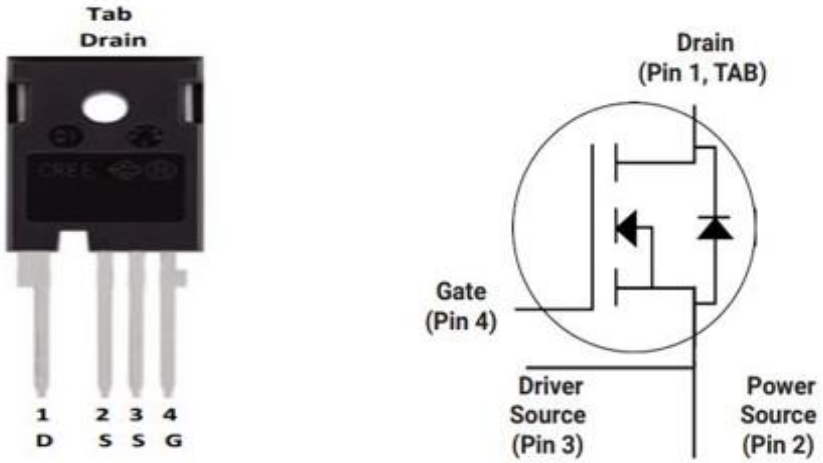

Figure 7-1: SiC MOSFETS Pin Configuration [65]

Appendix-A presents the maximum ratings and specifications of the SiC MOSFETS at room temperature. Other than the ratings and the pin configurations, the Cree's CGD15SG00D2 Gate driver's hardware is shown in *Figure 7.2*, whereas *Figure 7.3* presents the upper and lower sides of the driver.

Figure 7-2: Gate Driver Cree's CGD15SG00D2 [66]

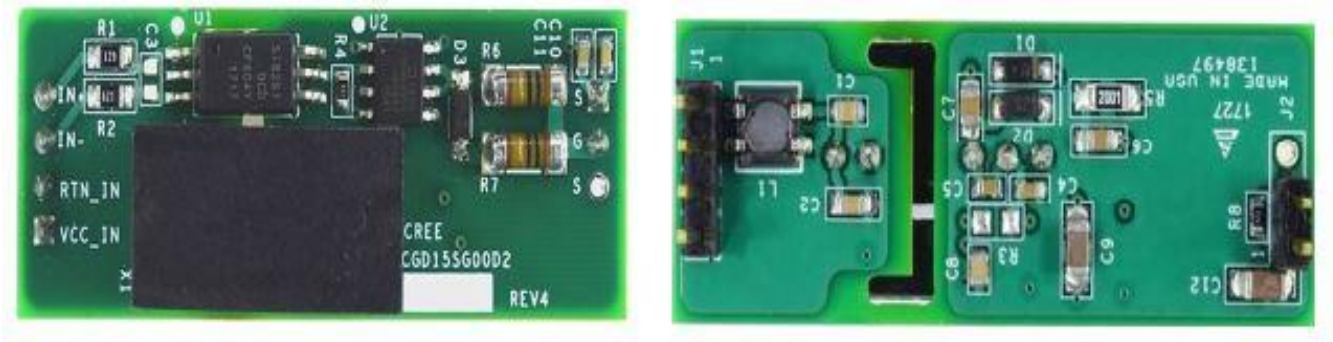

Figure 7-3: Upper and Lower View of CGD15SG00D2 [66]

There are six primary connections of Cree's gate-driven SiC MOSFETS. These connections are shown in *Figure 7.4* in tabular as well as pin connection form.

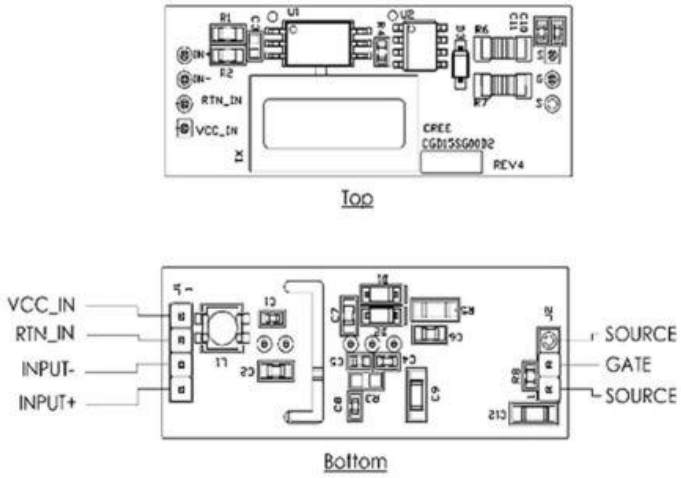

VCC_IN	12V Input
RTN_IN	12V Return
INPUT-	PWM Return
INPUT	PWM Input
Source	MOSFET Source
Gate	MOSFET GATE

Figure 7-4: Connections for Gate Driver CGD15SG00D2 [66]

Like every other MOSFETS, Cree's SiC MOSFETS also has some operating conditions listed in *Appendix-B.*

7.2. SIMPLE SWITCHING CIRCUIT WITH SERIES LOAD

This CKT is simply to test the gate driver with SiC to test the switching. A 22-ohm resistor is used in series with the input of the MOSFETS. To generate the PWM for the gate driver, we use Arduino mega 2560. An input DC source of 24 Volts and a switching frequency of 1 kHz. The circuit diagram is presented in *Figure 7.5*.

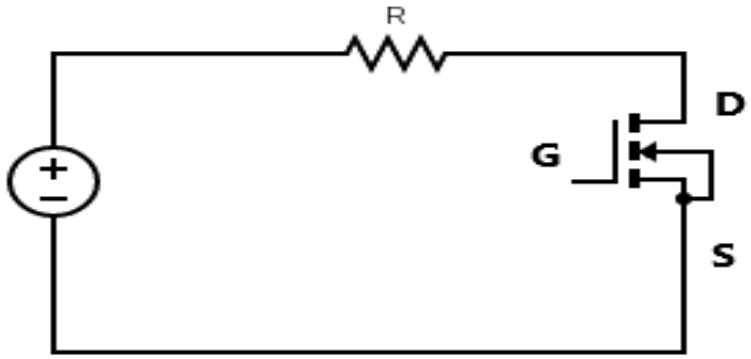

Figure 7-5: Circuit Diagram

The code through which the Arduino Mega 2560 is programmed and the PWM is generated for the Gate driver is shown in *(appendix D)*.

7.3. RESULTS

The designed hardware is tested, and the relevant results are obtained that are displayed in this section. First of all, the PWM is generated and obtained results are shown in *Figure 7.6*. The PWM is generated with peak amplitude of 4.8 Volts.

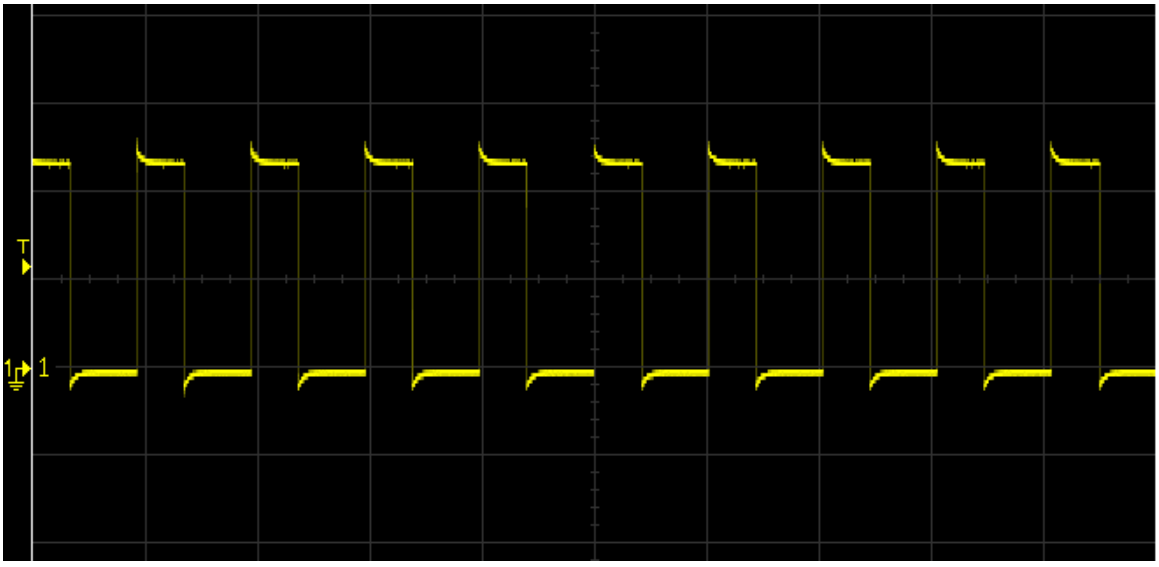

Figure 7-6: PWM Generated with peak Amplitude of 4.8 Volt

After the PWM generation, the Drain parameters are obtained through the simulations using an oscilloscope (CRO). The *Figure 7.7* shows the drain current captured at a peak of about 700mAmps; *Figure 7.8* shows the drain to source voltage (V_{DS}) that ranges from -1 Volts to +22 Volts. *Figure 7.9* shows the gate to source voltage (V_{GS}) with 5 Volt peak amplitude.

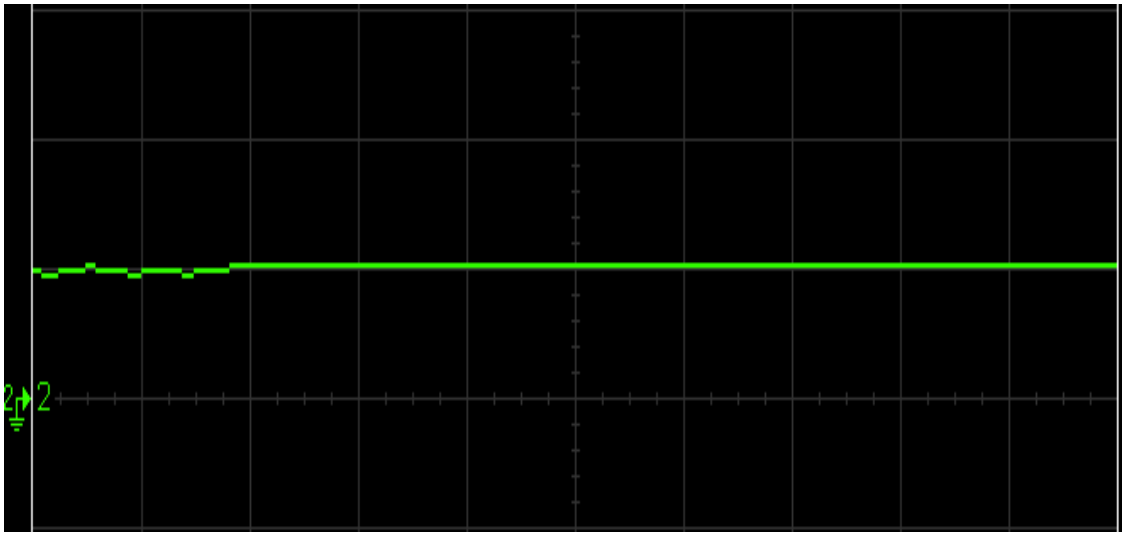

Figure 7-7: Drain Current with 700mA Peak

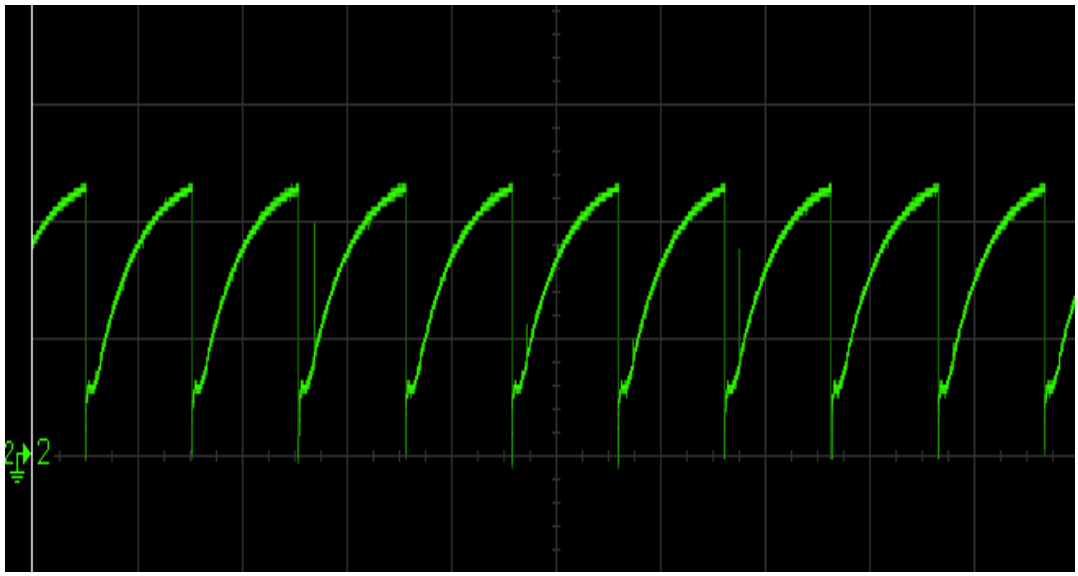

Figure 7-8 : Drain to Source Voltage from -1 to 22 Volts

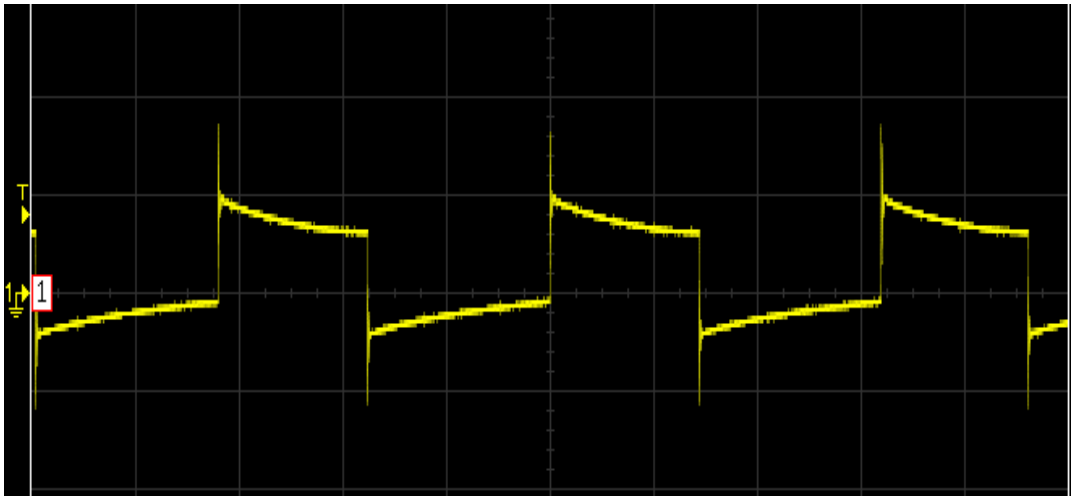

Figure 7-9: Gate to Source Voltage of Peak Amplitude of 5 Volts

We have used the Flir IR A315 camera to see the heat temperatures for both the SiC MOSFETS and Gate driver, which shows the switch has a high temperature of up to 94-degree Celsius and gate driver to 64-degree Celsius after 20 minutes of CKT running, which shows that it is best to use a heat sink for higher switching and voltage circuits. Figure 7.10 shows the peak temperature of SiC MOSFET of 94℃ & the gate driver with temperature of 64℃.

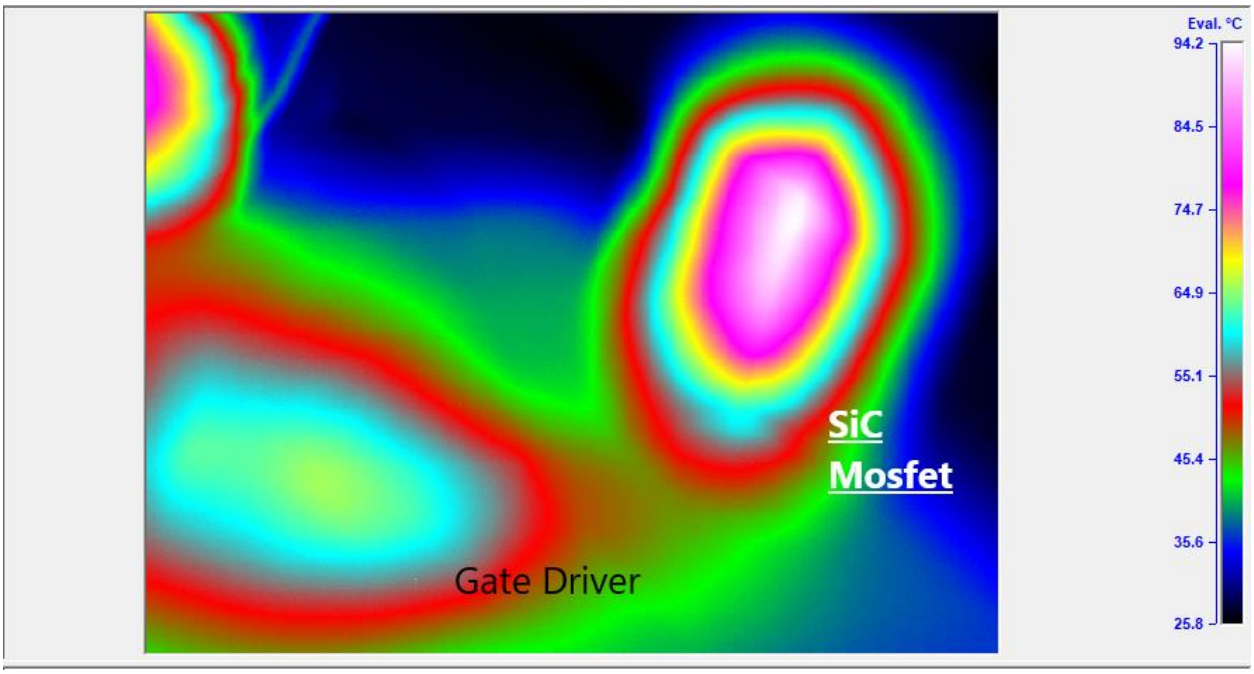

Figure 7-10: Temperature for SiC and Gate Driver

7.4. HALF-BRIDGE CIRCUIT USING COMMON SOURCE MODE

We will use the common source mode for a half-bridge CKT converter using four SiC switches and two gate drivers with a load resistance of 47 ohms, a DC source of 12 Volts, and a switching frequency of 1 kHz. But it was a problem to generate 4 PWMs for the switches. Arduino alone was not enough to generate perfect inverted PWMs and was not accurate. So, while I was searching for a better method, I came across an advantageous method from which we can quickly generate as many PWMs as we require by connecting Arduino with the Simulink. For that, we need to install two add-ons, namely MATLAB support for Arduino and Simulink support for Arduino. After that, we can use many ways to use Arduino with Simulink with just using the blocks and skipping the programming step for Arduino. But we need to add the gain up to 500 to get the required amplitude of 5 Volts for the PWM. The block diagram of the circuit is shown below. The circuit for half bridge is shown in the Figure 7.11.

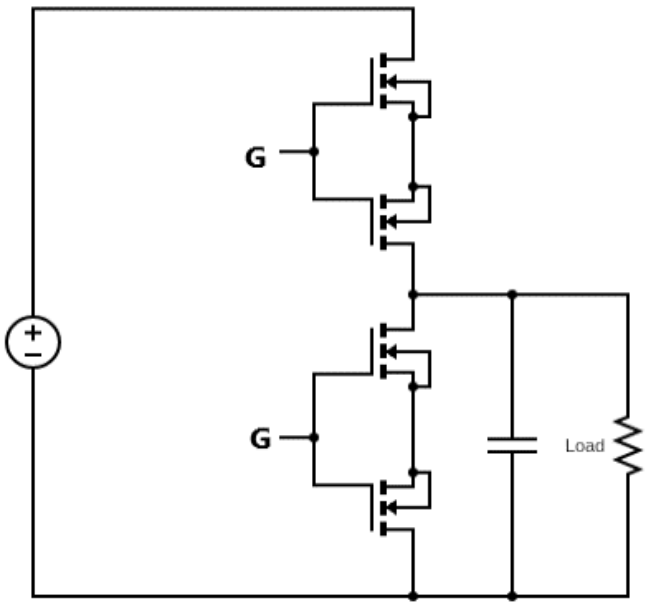

Figure 7-11: Circuit diagram for half bridge

The circuit is constructed in MATLAB Simulink for the simulations. The Circuit is for the PWM generation through Arduino. Figure 7.12 shows the PWM circuit.

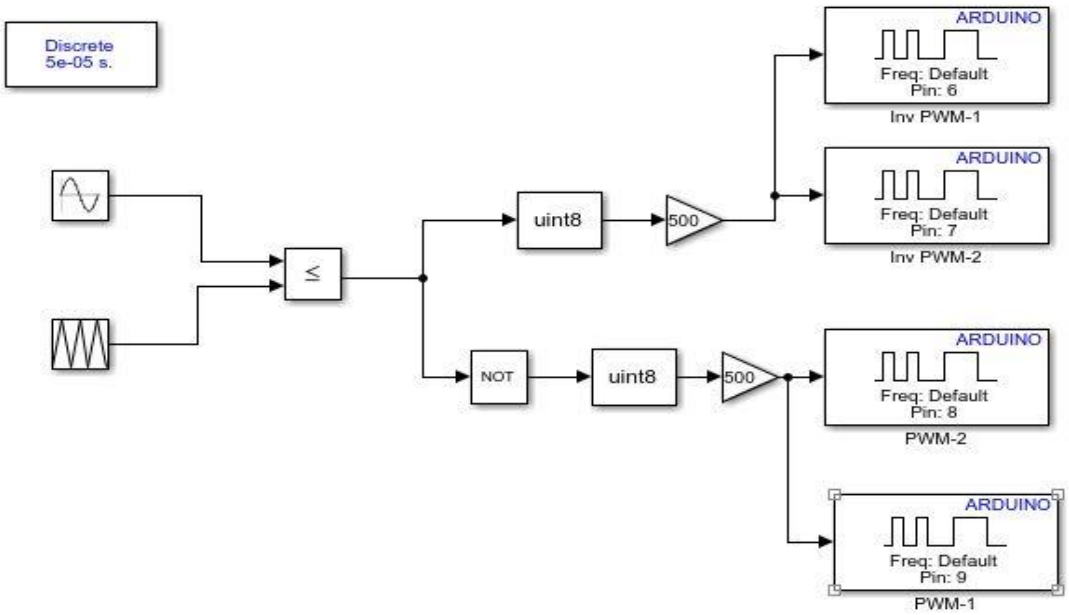

Figure 7-12: Simulink MATLAB Circuit for PWM through Arduino

7.5. RESULTS

The half-bridge common source circuit is simulated in Simulink , and the following shown results are obtained. The PWM generated through Arduino is shown in the figure 7.13 that is later on provided to 7 and 8 pins of Arduino.

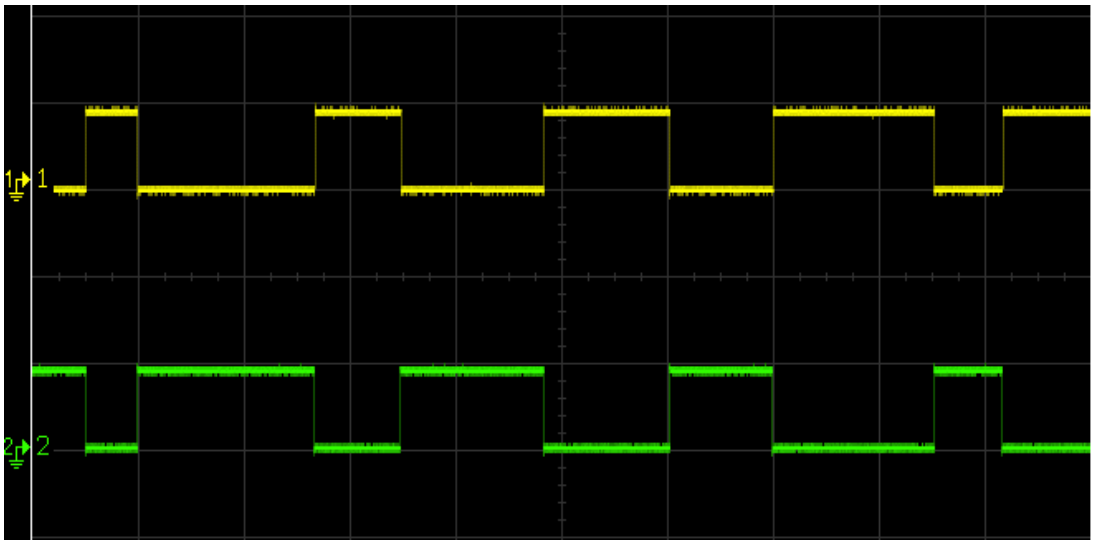

Figure 7-13: PWM from Arduino for Pin 7 and Pin 8

The current waveform is captured across the load and is presented in the figure 7.14. Load current has noise because of the many small wires use and the load current, which is very low because of the small input source voltage.

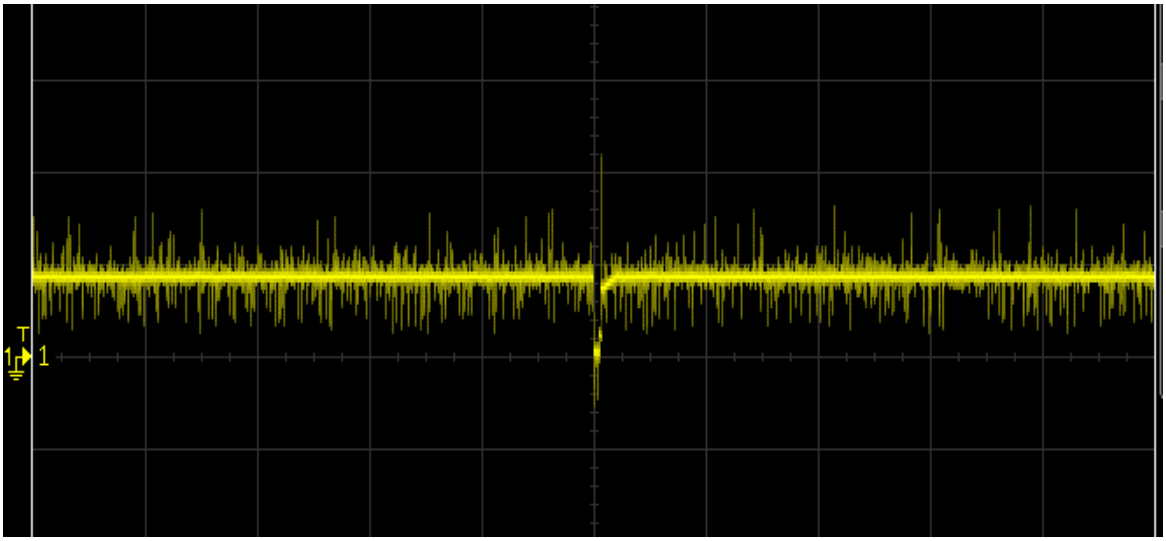

Figure 7-14: Load Current of 200 mAmp of Peak Current

The load voltage with the range 0 to 7.2 V is shown in figure 7.15.

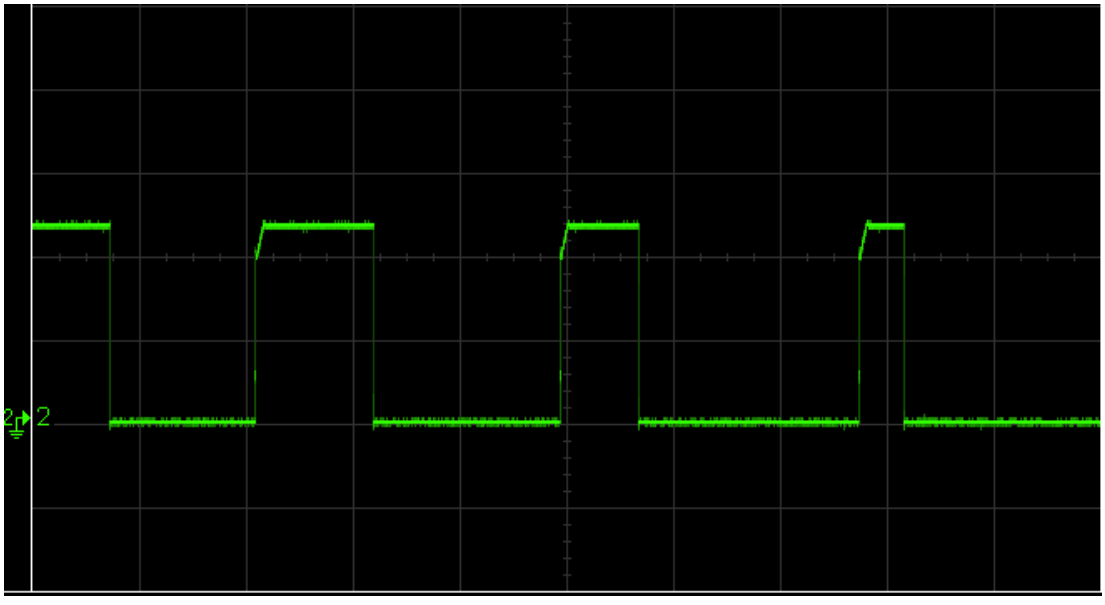

Figure 7-15: Load Voltage of Range 0 to 7.2 Volts

The V_{GS} and V_{SD} are presented in the figures 7.16 & 7.17 respectively. The V_{GS} is for the 1st and 4th switch, whereas the V_{SD} is for the 2nd and 3rd switch.

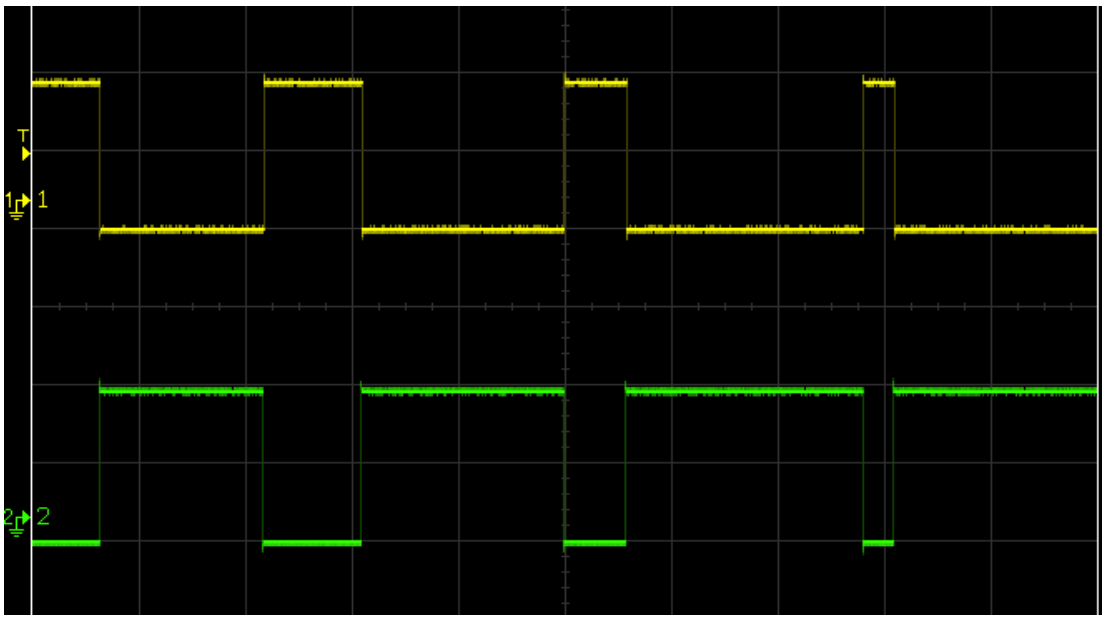

Figure 7-16: Gate to Source Voltage foe Switch 1 and Switch 4 of Peak amplitude 2 Volts

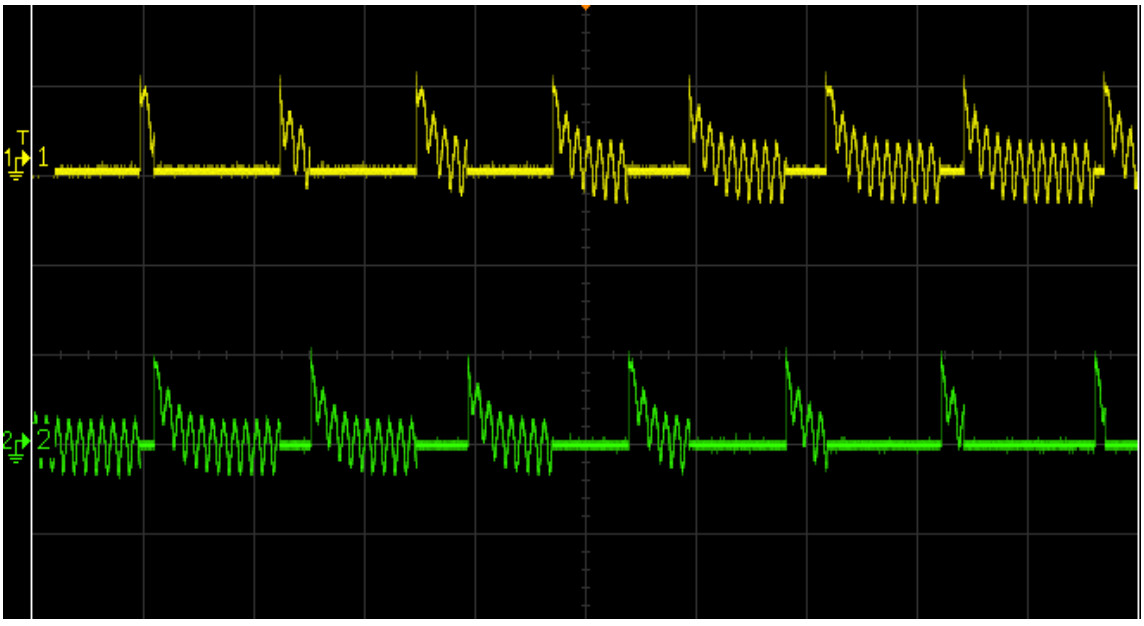

Figure 7-17: Source to Drain Voltage of Switch 2 and Switch 3 Acting on Diodes with Peak Amplitude of 0.2 Volts

8. CONCLUSION

This section of the thesis concludes the whole dissertation and work performed in the experiences related to the thesis. Moreover, it elaborates on some of the scopes of further study that can be a part of this thesis's future.

The dissertation includes SiC and its compatible CSCs. It involves its introduction, related literature, applications, limitations, along with the hardware and software circulation of SiC switch-based half-bridge, full-bridge, and three-phase power inverter. These circuits and simulations prove the efficient working of the SiC switches and current sources. The simulation and PCB are designed using LTspice and Easy EDA software to efficiently circuit and simulate tools. After the practical results, the hardware is designed and tested for the desired output, and it can be seen from the results that the SiC is a powerful addition to power electronics. It is the perfect choice for the power circuits like three-phase inverters, power modules, etc. In short, the SiC is an efficient, fast switching device that contains many properties that are beneficial in many applications, especially high-power applications for their capability to work with high power and high frequency circuits. The work in this thesis provides a strong base for the future work of hardware in this topic. The switches and gate drivers are selected and tested with the ready to print PCB designs and simulations, to implement them in the hardware for all the discussed circuits of half bridge, full bridge and three phase CSIs in the future research work.

REFERENCES

[1]. Henk Nijmeijer, and Arjan van der Schaft, "Nonlinear Dynamical Control Systems," *SpringerLink*, pp. 423 – 426, 1990.

[2]. Rudrarju, and Sai Nikitha," Scaling of an Ion Implanted SiC (SiC) Based Mesfet," *CSUN – Scholar Works*, 2016.

[3]. Alix Paultre, *A Brief History of SiC*, Power Electronics News, 2018.

[4]. Trer R. J., "The Operation of Microwave Power Amplifiers Fabricated from Wide Bandgap Semiconductors," *IEEE MTT-S Digest*, pp. 45 - 48, 1997.

[5]. Amy Tikkanen, *SiC – Chemical Compound*, Britannica, 2008.

[6]. Rich Miron, *SiC (SiC): History and Applications*, Digi-Key Electronics, 2016.

[7]. A. Elasser, and T. P. Chow, "SiC Benefits and Advantages for Power Electronics Circuits and Systems," *Proceedings of IEEE*, vol. 90, pp. 969 – 986, 2002.

[8]. S. Ede, J. U. Odo, I. Adiele, J. Ani, C. W. Onyia, and B. A. Okorie, "Effects of SiC (SIC) Nano Particulates Addition on Mechanical Properties of Aa 2618 Alloy," *Semantic Scholar*, 2015.

[9]. R. Kirschman, "High-Temperature SiC Electronic Devices (Westinghouse)," *High-Temperature Electronics*, Edition: Wiley IEEE Press, pp. 83 – 86, 1999.

[10]. J. W. Palmour, R. Singh, R. C. Glass, O. Kordina, and C. H. Carter, "SiC for Power Devices," *IEEE International Symposium Journal on Power Semiconductor Devices and IC's, ISPSD '97*, pp. 25 – 32, 1997.

[11]. R. Strzelecki, and G. Benysek, "Power Electronics in Smart Electrical energy Network," *Dordrecht: Springer*, 2008.

[12]. B. J. Baliga, *SiC Power Devices*, River Edge, NJ, USA: World Scientific, 2006.

[13]. B. J. Baliga, "Fundamentals of Power Semiconductor Devices," *Springer*, 2008.

[14]. Xiangxiang Fang, "Characteristics and Modeling of SiC Power MOSFETSs," *Master's Thesis for Master of Science, The Ohio State University*, 2012.

[15]. STMicroelectronics, *Tech Comparison, Breakthrough in Power Electronics*, 2014.

[16]. D. Othman, S. Lefebvra, M. Berkani, Z. Khatir, A. Ibrahim, and A. Bouzourene, "Robustness of 1.2 kV SiC MOSFETS Devices," *Microelectronics Reliability*, vol. 53, no. 9, pp. 1735 – 1738, 2013.

[17]. X. Zhang, M. Chen, N. Zhu, and D. Xu, "A Self-Adaptive Blanking Circuit for IGBT Short-Circuit Protection Based on VCE Measurement," *IEEE Energy Conversion Congress and Exposition (ECCE)*, pp. 4125 – 4131, 2015.

[18]. N. Mohan, T. M. Undeland, and W. P. Robbins, "Power Electronics: Converters, Applications, and Design," *3rd Edition Hoboken, N. J. Wiley*, 2003.

[19]. M. Joko, A. Goto, M. Hasegawa, S. Miyahara, and H. Murakami, "Snubber Circuit to Suppress the Voltage Ringing for SiC Device," *PCIM Europe 2015: International Exhibition and Conference for Power Electronics, Intelligent Motion, Renewable Energy, and Energy Management*, pp. 1 – 6, 2015J. Dodge, "Power MOSFETS Tutorial," *Application Note APT – 0403 Rev. B – Advanced Power Technology*, 2006.

[20]. P. Vaculik, "The Experience with SiC MOSFETS and Buck Converter Snubber Design," *International Journal of Electrical, Computer, Energetic, Electronic, and Communication Engineering*, vol. 8, Edition: International Science Index, pp. 49 – 54, 2014.

[21]. K. Vechalapu, S. Bhattacharya, and E. Aleoiza, "Performance Evaluation of Series Connected 1700V SiC MOSFETS Device," *Wide Bandgap Power Devices and Applications (WiPDA), IEEE 3rd Workshop*, pp. 184 – 191, 2015.

[22]. Masayuki Imaizumi, Yoichiro Tarui, Shin Ichi Kinouchi, Hiroshi Nakataka, Yukisyasu Nakao, Tomokatsu Watanabe, Keiko Fujihira, Naruhisa Miura, Tetsuya Takami, and Tatsuo Ozeki, "Switching Characteristics of SiC – MOSFETS and SBD Power Modules," vol. 527 – 529, pp. 1289 – 1292, 2006.

[23]. *Compare D-MOSFETS and E-MOSFETS Considering Construction and Characteristics*, Ques10, 2020.

[24]. Joseph Fabre, Philippe Ladoux, and Michel Piton, "Characterization and Implementation of Dual-SiC MOSFETS Modules for Future Use in Traction Converters," *IEEE Transactions on Power Electronics*, vol. 30, no. 8, pp. 4079 – 4090, 2015.

[25]. J. Dodge, "Power MOSFETS Tutorial," *Application Note APT – 0403 Rev. B – Advanced Power Technology*, 2006.

[26]. V. Barkhordarian, "Power MOSFETS Basics," *Alpha & OMEGA – Semiconductor*, 2009.

[27]. T. Kimoto, and J. A. Cooper, "Fundamentals of SiC Technology: Growth, Characterization, Devices, and Applications," *Somerset: Somerset: Wiley*, 2014.

[28]. S. M. Muyeen, "Wind Energy Conversation Systems: Technology and Trends," *Technology and Trends - Springer*, pp. 12 – 13, 2012.

[29]. Vitor Monteiro, J. G. Pinto, Bruno Exposto, and Joao Afonso, "Comprehensive Comparison of a Current-Source and a Voltage-Source Converter for Three-Phase EV Fast Battery Charges," *9th Internation Conference on Compatibility and Power Electronics (CPE)*, 2015.

[30]. J. Liu, K. L. Wong, A. Allen, and J. Mookken, "Performance Evaluations of Hard-Switching Interleaved DC/DC Boost Converter with New Generation SiCs," *Darnell's Power Forum*, 2013.

[31]. Thomas Friedli, Simon D. Round, Dominik Hassler, and Johann W. Kolar, "Design and Performance of a 200 kHz All-SiC JFET CSC," *IEEE Industry Applications Society Annual Meeting*, 2008.

[32]. Erik Velander, Lennart Kruse, Stephan Meier, Andreas Lofgren, Thomas Wiik, Hans-Peter Nee, and Diane-Perle Sadik, "Analysis of Short Circuit Type II and III of High Voltage SiC MOSFETSs with Current Source gate Drive Principle," *IEEE 8th International Power Electronics and Motion Control Conference (IPEMC – ECCE Asia)*, 2016.

[33]. Maurizio Di Paolo Emili, "SiC MOSFETSs Bring Disruptive Breakthroughs to Power Systems," *EETimes*, 2019.

[34]. *Physical Properties and Characteristics of SiC*, SiC – Rohm Semiconductors, 2021.

[35]. C. Klumpner, "A New Single-Stage CSI for Photovoltaic and Fuel Cell Applications using Reverse Blocking IGBTs," *IEEE Power Electronics Specialists Conference*, 2007.

[36]. Xiangyu Han, Liran Zheng, Rajendra Prasad Kandula, Karthik Kandasamy, Deepak Divan, and Maryam Saeedifard, "Characterization of 3.3 kV Reverse-Blocking SiC Modules for Use in Current-Source Zero-Voltage-Switching Converters," *IEEE Transactions on Power Electronics*, vol. 36, no. 1, pp. 876 - 887, 2021.

[37]. Xiangyu Han, Liran Zheng, Rajendra Prasad Kandula, Karthik Kandasamy, Deepak Divan, and Maryam Saeedifard, "Characterization of 3.3 kV Reverse-Blocking SiC Modules for Use in Current-Source Zero-Voltage-Switching Converters," *IEEE Transactions on Power Electronics*, vol. 36, no. 1, pp. 876 - 887, 2021Aniruddh Marellapudi, Michael J. Mauger, Prasad Kandula, and Deepak Divan, "Enabling High Efficiency in Low Voltage Soft Switching CSCs," *IEEE Energy Conversion Congress and Exposition (ECCE)*, 2020.

[38]. V. Jayaseelan, K. Kalalchelvan, M. Kannan, and S. Vijay Ananth," Influence of Friction factor on Extrusion Process – Extrusion Characteristics of Al/SiC by Different Manufacturing Process," *International Journal of Applied Engineering Research, DinDigul*, vol. 1, no. 1, pp. 194 - 199, 2010.

[39]. G. S. Gupta, P. Vasanth Kumar, V. R. Rudolph, and M. Gupta, "Heat-Transfer Model for the Acheson Process," *SpringerLink – Metallurgical and Materials Transactions A*, vol. 32, pp. 1301 - 1308, 2001.

[40]. Bilijana Babic, Dusan Bucevan, Ana Radosavljevic – Mihajlovic, Anja Dosen, Jelena Zagorac, Jelena Pantic, and Branko Matovic, ”New Manufacturing Process for Nanometric SiC,” *ECERS – Journal of European Ceramic Society*, vol. 32, no. 9, pp. 1901 - 1906, 2012.

[41]. Byrappa, Kullaiah, Ohachi, and Tadashi, "Crystal Growth Technology," *SpringerLink - Science and Business Media*, 2018.

[42]. Lely, Jan Anthony, Emmasingel, and Eindhoven, "Sublimation Process for manufacturing SiC Crystals," 1958.

[43]. Alireza Kouchaki, and Morten Nymand," High-Efficiency Three-Phase Power Factor Correction Rectifier Using SiC Switches," *19th European Conference on Power Electronics and Applications (EPE'17 ECCE Europe)*, 2017.

[44]. Paco Bogonez-Franco, and Josep Balcells Sendra," EMI Comparison between Si SiC Technology in a Boost Converter," *International Symposium on Electromagnetic Compatibility – EMC EUROPE*, 2012.

[45]. Rohm Semiconductor, "SiC Power Devices and Modules, Application Note," 2014.

[46]. Masayuki Imaizumi, Yoichiro Tarui, Shin Ichi Kinouchi, Hiroshi Nakatake, Yukiyasu Nakao, Tomokatsu Wantanbe, Keilo Fujihira, Naruhisa Miura, Tetsuya Takami, and Tatsuo Ozeki, "Switching Characteristics of SiC MOSFETS and SBD Power Modules," Material Science Forum *Edition*, vol. 527-529, pp. 1289 - 1292, 2006.

[47]. J. Fabre, P. Ladoux, and M. Piton, "Characterization and Implementation of Dual SiC MOSFETS Modules for Future Use in Traction Converters," *IEEE Transaction on Power Electronics*, vol. 30, pp. 4079 - 4090, 2015.

[48]. Kai Sun, Hogfei Wu, Juejing Lu, Yan Xing, and Lipei Huang, "Improved Modeling of Medium Voltage SiC MOSFETS Within Wide Temperature Range," *IEEE Transaction on Power Electronics*, vol. 29, no. 5, pp. 2229 - 2237, 2014.

[49]. Shi Pu, Fei Yang, Bhanu Teja Vankayalapati, Enes Ugur, Chi Xu, and Bilal Akin, "A Practical On-Board SiC MOSFETS Condition Monitoring Technique for Aging Detection," *IEEE Transactions n Industry Applications*, vol. 56, no. 3, pp. 2828 - 2839, 2020.

[50]. I. Omura, and W. Fichtner, "Numerical Study of Reverse Blocking Switching Devices in CSIs, in Comparison with Normal Devices in CSIs and Voltage Source Inverters," *9th International Symposium on Power Semiconductor Devices and IC's*, 2002.

[51]. Vincenzo Madonna, Giovanni Migliazza, Paolo Giangrande, Emilio Lorenzani, Giampaolo Buticchi, and Michael Galea, "The Rebirth of the CSI: Advantages for Aerospace Motor Design," *IEEE Industrial Electronics Magazine*, vol. 13, no. 4, 2019.

[52]. *What is CSI: Working and Its Applications*, ELPROCUS, 2020..

[53]. *BaSiCs of SiC: Evolution of SiC in Power Electronics*, Wolfspeed – A Cree Company, 2019.

[54]. Ranbir Singh, "Reliability and Performance Limitations in SiC Power Devices," *Microelectronics Reliability*, vol. 46, no. 5 - 6, pp. 713 - 730, 2006.

[55]. Shiqi Ji, Sheng Zheng, Fei Wang, and Leon M. Tolbert, "Temperature-Dependent Characterization, Modeling, and Switching Speed Limitation Analysis of Third Generation 10 kV SiC MOSFETS," *IEEE Transactions on Power Electronics*, vol. 33, no. 5, pp. 4317 - 4327, 2018.

[56]. Maurizio Di Paolo Emilio, *The Importance of SiC Semiconductors for Energy Efficiency*, EETimes, 2020.

[57]. Chin Chang, and G. Bruning, "Voltage-fed half-bridge resonant converter for multiple lamp independent operations," *Conference Record of the 2001 IEEE Industry Applications Conference. 36th IAS Annual Meeting (Cat. No.01CH37248)*, vol. 1, pp. 218 – 222, 2001.

[58]. E. Adib, and H. Farzanehfard, "Zero-Voltage Transition Current-Fed Full-Bridge PWM Converter," in *IEEE Transactions on Power Electronics*, vol. 24, no. 4, pp. 1041 – 1047, 2009.

[59]. PRASANNA, U. R. and RATHORE, A. K. Analysis, "Design, and Experimental Results of A Novel Soft-Switching Snubberless Current-Fed Half-Bridge Front-End Converter-Based Inverter," *IEEE Transactions on Power Electronics*, vol. 28, no. 7, p. 3219 – 3230, 2013.

[60]. C. F. Moraes, E. G. Carati, J. P. da Costa, R. Cardoso, and C. M. d. Oliveira Stein, "Active-Clamped Zero-Current Switching Current-Fed Half-Bridge Converter," in *IEEE*

Transactions on Power Electronics, vol. 35, no. 7, pp. 7100-7109, July 2020, doi: 10.1109/TPEL.2019.2959447.

[61]. Hang Dai, Thomas M. Jahns, Renato A. Torres, Mingda Liu, Bulent Sarlioglu, and Steven Chang, "Development of High-Frequency WBG Power Modules with Reverse-Voltage-Blocking Capability for an Integrated Motor Drive using a Current-Source Inverter," *Wisconsin Electric Machines and Power Electronics Consortium (WEMPEC)*.

[62]. Alec Dorling, "SPICS: Software Process Improvement and Capability Determination," *SpringerLink – Software Quality Journal*, vol. 2, pp. 209 – 224, 1993.

[63]. John C. Ksander, Sarah M. Kark, and Christopher R. Madan, "Breathe Easy EDA: A MATLAB Toolbox for Psychophysiology Data Management, Cleaning, and Analysis," *PMC – F1000 Research*, vol. 7, no. 216, 2018.

[64]. CREE, "CGD15SG00D2 – Gate Driver for Cree's Generation 3 (C3M^{TM}) SiC MOSFETS," 2020.

[65]. CREE, "SiC Power MOSFETS – C3M^{TM} MOSFETS Technology," 2020.

[66]. Mikael Ostling, Reza Ghandi, Carl-Mikael Zetterling, "SiC Power Devices – Present Status, Applications, and Future Perspective," *IEEE 23rd International Symposium on Power Semiconductor Devices and ICs*, 2011.

APPENDICES

APPENDIX A: MAXIMUM RATINGS OF SiC MOSFETS

Maximum Ratings of SiC MOSFETS at T_C = 20°C [91]

Sr. No.	Symbol	Parameter	Value	Unit	Test Conditions
1.	V_{DSmax}	Drain – Source Voltage	1200	V	V_{GS} = 0V, I_D = 100 μA
2.	V_{GSmax}	Gate – Source Voltage (dynamic)	-8/+19	V	AC (f >1 Hz)
3.	V_{GSop}	Gate – Source Voltage (static)	-4/+15	V	Static
4.	I_D	Continuous Drain Current	66	A	V_{GS} = 15V, T_C = 25°C
			48		V_{GS} = 15V, T_C = 100 °C
5.	$I_{D(pulse)}$	Pulsed Drain Current	100	A	Pulse width t_P limited by T_{jmax}
6.	P_D	Power Dissipation	326	W	T_C = 25 °C, T_J = 175 °C
7.	T_J, T_{stg}	Operating Junction and Storage Temperature	-40 to +175	°C	
8.	T_L	Solder Temperature	260	°C	1.6mm (0.063”) from case for 10s

APPENDIX B: OPERATING CONDITIONS FOR GATE DRIVER

Operating Conditions of Gate Driver CGD15SG00D2 [92]

Operating Conditions						
Sr. No.	**Symbol**	**Parameter**	**Min**	**Typical**	**Max**	**Unit**
1.	V_S	Power Supply Voltage	11	12	12.5	V
2.	V_{iH}	Input Threshold Voltage HIGH	10		15	V
3.	V_{iL}	Input Threshold Voltage LOW	0		1	V
4.	I_{o_pk}	Output Peak Current	-9		9	A
5.	P_{O_AVG}	Output Power per Gate	1			W
6.	V_{ISOL}	Input to Output Isolation Voltage		±1700		V
7.	dv/dt	Rate of Change of Output to Input Voltage		50,000		V/μs
8.	W	Weight		9		g
9.	MTBF	Operating Temperature		-35 TO 85		°C
10.	Top	Storage Temperature		-40 TO 85		°C

APPENDIX C: HARDWARE CIRCUIT FOR TESTING SINGLE SiC MOSFETS

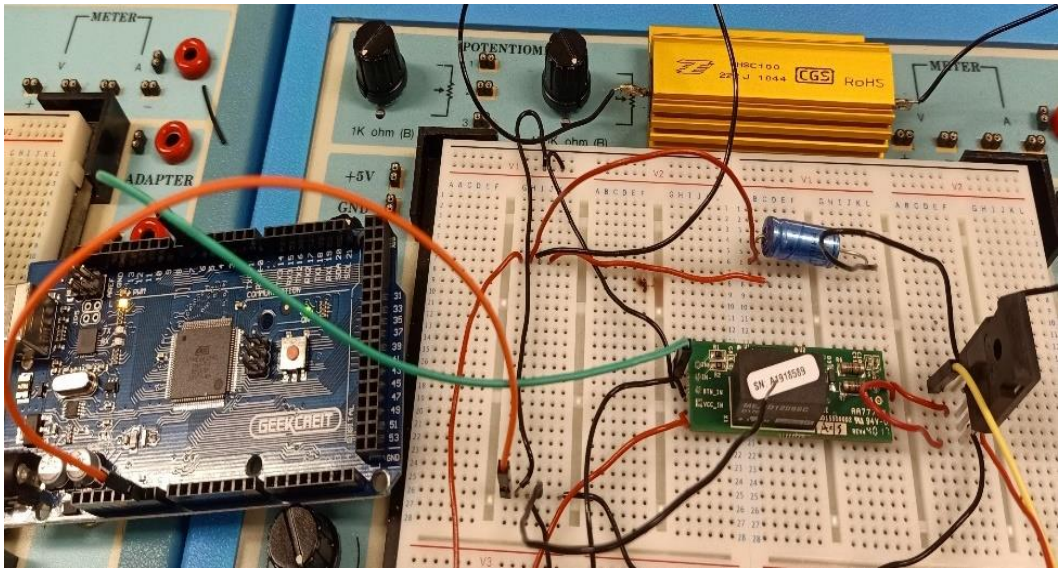

Single SiC MOSFETS Testing (Circuit Hardware)

APPENDIX D: PWM GENERATION CODE FOR GATE DRIVER

```
/*
  Generating PWM at pin # 6 on Arduino MEGA 2560

  */
int PWM1 = 6;
void setup()
{

}
void loop() {
  // Sweep pin value from min (0) to max (255):
  for (int change = 0 ; change <= 255; change += 1)
  {
    // write value to the assigned pin:
    analogWrite(PWM1, fadeValue);
    // wait for 30 milliseconds
    delay(30);
  }

  // Sweep back from 255 to 0:
  for (int change = 255 ; change >= 0; change -= 1) {
    analogWrite(PWM1, change);
    // wait for 30 milliseconds
    delay(30);
  }
}
```

APPENDIX E: HALF-BRIDGE COMMON SOURCE CIRCUIT

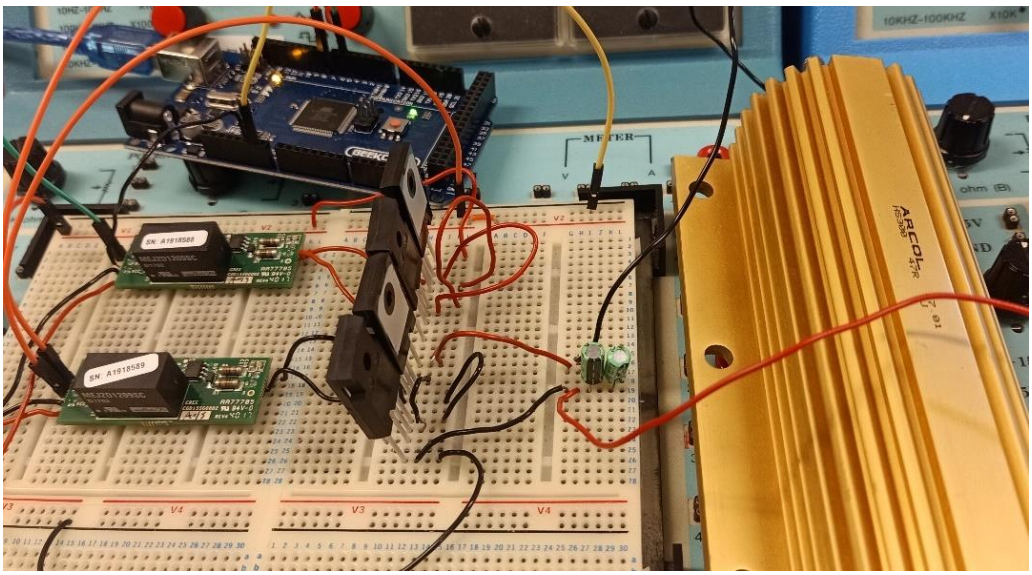

Half-Bridge Common Source Circuit